1  Single-cell characterization of the human C2 dorsal root ganglion recovered from C1-2
2  arthrodesis surgery: implications for neck pain

3  Short title: Characterization of the human C2 DRG

4  Asta Arendt-Tranholm[1], Ishwarya Sankaranarayanan[1], Cathryn Payne[2], Marisol Mancilla
5  Moreno[1], Khadijah Mazhar[1], Natalie Yap[2], Abby P. Chiu[2], Allison Barry[1], Pooja P. Patel[1], Nikhil
6  N. Inturi[1], Diana Tavares Ferreira[1], Anubhav Amin[2], Mahesh Karandikar[2], Jeffrey G. Jarvik[2,4,6],
7  Judith A. Turner[5,6], Christoph P. Hofstetter[2], Michele Curatolo[3,6], Theodore J. Price.[1]

8  [1] Center for Advanced Pain Studies, Department of Neuroscience, University of Texas at Dallas,
9  Richardson, TX, USA.

10  [2] Department of Neurological Surgery, University of Washington, Seattle WA, USA.

11  [3] Department of Anesthesiology and Pain Medicine, University of Washington, Seattle WA, USA.

12  [4] Department of Radiology, University of Washington, Seattle WA, USA.

13  [5] Department of Psychiatry & Behavioral Sciences, University of Washington, Seattle WA, USA.

14  [6] The University of Washington Clinical Learning, Evidence and Research (CLEAR) Center for
15  Musculoskeletal Disorders.

16

17  **Correspondence**:

18  Theodore J. Price, 800 W Campbell Rd, BSB 14.102, Richardson, TX, 75080 USA. 972-883-
19  4311. Theodore.price@utdallas.edu

27  Conflict of Interest Statement: T.J.P. is a co-founder and holds equity in 4E Therapeutics,
28  NuvoNuro, PARMedics, and Nerveli. T.J.P. has received research grants from AbbVie, Eli Lilly,
29  Grünenthal, Evommune, Hoba Therapeutics, and The National Institutes of Health. M.C. is the
30  chief medical officer and holds equity in 4E Therapeutics.

31

32

33

34

1

**Abstract**

Neurons in the dorsal root ganglion (DRG) receive and transmit sensory information from the tissues they innervate and from the external environment. Upper cervical (C1-C2) DRGs are functionally unique as they receive input from the neck, head, and occipital cranial dura, the latter two of which are also innervated by the trigeminal ganglion (TG). The C2 DRG also plays an important role in neck pain, a common and disabling disorder that is poorly understood. Advanced transcriptomic approaches have significantly improved our ability to characterize RNA expression patterns at single-cell resolution in the DRG and TG, but no previous studies have characterized the C2 DRG. Our aim was to use single-nucleus and spatial transcriptomic approaches to create a molecular map of C2 DRGs from patients undergoing arthrodesis surgery with ganglionectomy. Patients with acute (<3 months) or chronic (≥3 months) neck pain were enrolled and completed patient-reported outcomes and quantitative sensory testing prior to surgery. C2 DRGs were characterized with bulk, single nucleus, and spatial RNA sequencing technologies from 22 patients. Through a comparative analysis to published datasets of the lumbar DRG and TG, neuronal clusters identified in both TG and DRG were identified in the C2 DRG. Therefore, our study definitively characterizes the molecular composition of human C2 neurons and establishes their similarity with unique characteristics of subsets of TG neurons. We identified differentially expressed genes in endothelial, fibroblast and myelinating Schwann cells associated with chronic pain, including *FGFBP2, C8orf34* and *EFNA1* which have been identified in previous genome and transcriptome wide association studies (GWAS/TWAS). Our work establishes an atlas of the human C2 DRG and identifies altered gene expression patterns associated with chronic neck pain. This work establishes a foundation for the exploration of painful disorders in humans affecting the cervical spine.

**Introduction**

Since the introduction of single cell and spatial sequencing technologies, a major goal of the somatosensation and pain neuroscience fields has been to characterize dorsal root ganglion (DRG) and trigeminal ganglion (TG) cells with molecular precision (Renthal et al., 2021). Great progress has been made in this area using rodent DRG and TG neurons where we now have comprehensive cell censuses from development to adulthood and including many chronic pain models (Usoskin et al., 2015; Zeisel et al., 2018; Renthal et al., 2020; Sharma et al., 2020). Similar progress has been made in characterizing the human DRG and TG where we also now have spatial and single cell sequencing datasets that demonstrate that there are between 12 and 18 subtypes of sensory neurons in the adult human, lumbar DRG (Nguyen et al., 2021; Tavares-Ferreira et al., 2022; Jung et al., 2023; Bhuiyan et al., 2024; Yu et al., 2024). Subtypes of human TG neurons have also been characterized (Yang et al., 2022), although to a lesser extent than the progress that has been made on lumbar DRGs. These studies have revealed full transcriptomes of neuronal cell types in multiple species and a harmonized atlas across species has recently been built (Bhuiyan et al., 2024). Important species differences have also been found. One major difference between humans and rodents is the more expansive expression of the capsaicin and noxious heat receptor TRPV1 in human DRG neurons (Shiers et al., 2020; Shiers et al., 2021; Tavares-Ferreira et al., 2022). Another is the lack of a clear distinction between peptidergic and non-peptidergic nociceptors in human DRG (Shiers et al., 2020; Shiers et al., 2021) and the identification of unique subsets of human DRG neurons (Tavares-Ferreira et al., 2022; Yu et al., 2024).

A key gap in knowledge is a lack of information about DRGs at the cervical level in humans. These DRGs, at the C1 and C2 level, are functionally and anatomically interesting because they innervate structures like skin, muscle and bone, but also the occipital portion of the cranial meninges (Keller et al., 1985; Noseda et al., 2019). The rest of the cranial meninges is innervated by the TG from the V1 subdivision of that ganglia. Presumably, DRG neurons in the C2 DRG would share characteristics of both DRG and TG neurons, but this hypothesis has never been addressed in humans. Another important gap in knowledge pertains to a common and disabling painful disorder – chronic neck pain. Neck pain is an important cause of disability world-wide; existing treatments are sparse and mostly lack an evidence base for their clinical use (Safiri et al., 2020; Wu et al., 2024). The C2 DRG innervates the atlantoaxial joint, a known originator of neck pain in osteoarthritis, and structures of the cervical spine that can be acutely injured after a fall. In addition, changes to the C2 DRG may be a source of pain. During C1-2 fusion surgeries, this DRG can be resected as part of clinical care.

The work described here had two primary goals. The first was to characterize the transcriptome of cells in the human C2 DRG using single cell and spatial transcriptomic techniques with the purpose of addressing how neurons in these ganglia relate to previous findings in lumbar DRG and TG of humans. The second goal was to ascertain whether the transcriptomes of these cells were altered in samples from people who suffer from chronic neck pain, compared to those with acute pain. This would address the lack of understanding of the transcriptional mechanisms underlying chronic neck pain, potentially identifying novel molecular targets to treat this burdensome condition.

Here we describe the first analysis of the human C2 DRG at single cell resolution. Our work demonstrates that there are similarities to both the lumbar DRG and TG in the human C2 DRG, consistent with its unique anatomical innervation pattern. The removal of these DRGs

3

104   during C1-2 fusion surgeries, performed to treat either an acute cervical spine injury or chronic
105   neck pain, provided an opportunity to examine changes in gene expression that might be linked
106   to chronic neck pain. We found several endothelial, fibroblast and Schwann cell-related genes
107   that were associated with chronic neck pain, and relatively few changes in neuronal
108   transcriptomes. Altogether, our findings enhance our knowledge of the molecular makeup of
109   human DRGs, expanding our understanding to the cervical level, and give insight into potential
110   mechanisms of chronic neck pain.

111   **Results**

112   ***Characterization of the human C2 DRG with single nucleus sequencing***

113   We used single-nucleus RNA sequencing (snRNA-seq) to characterize the molecular
114   composition of the C2 DRG. DRGs from 12 patients were included in this analysis, 7 DRGs from
115   patients with acute injury and 5 DRGs from patients with chronic pain. Nuclei were isolated from
116   hDRGs and fixed and barcoded   using the 10X flex kit to facilitate single-nucleus resolution
117   RNA expression data. We imposed cutoffs of 500 genes and 7.5% mitochondrial-RNA (mtRNA)
118   and obtained a minimum of 129 nuclei per sample. Two rounds of sequencing were performed
119   with more nuclei obtained per sample in the initial run, therefore the RunHarmony tool from the
120   Seurat package was used to merge and integrate the data. Using the FindClusters tool of the
121   Seurat package, we identified 18 unique cell clusters (Fig 1A-B). Expression of neuronal
122   (*SNAP25/PRPH*) and non-neuronal (*MPZ/COL1A1/FABP7*) marker genes correlated with
123   distinct groupings in the UMAP (Fig 1C-D). Representation from all samples was confirmed in
124   all neuronal clusters, however, the non-neuronal cells were largely collected in one run as
125   observed in Figure 1B. We suggest the variability in cell subtype recovery was due to technical
126   variation in the dissociation process. The data was subset into neuronal and neuronal groups, to
127   characterize subclusters in greater detail.

128       Fourteen non-neuronal cell clusters were identified as seen in Figure 1E. Marker gene
129   expression suggested several of these clusters were of the same non-neuronal cell type (Fig
130   1F). Expression of *COL1A1, PODN* and *DCN* was distinct in clusters 0, 3, 6, 7, and 11,
131   indicating fibroblast populations. Clusters 4 and 13 exhibited expression of *CD14* and *CD163*
132   indicating immune cell subtypes. Clusters 9 and 10 were identified as Schwann cells based on
133   *MLIP* and *PRX* expression. Clusters 1, 5 and 8 showed variable but distinct expression of
134   *NCAM1* and *FABP7*. Cluster 5 was unique in expressing *SERPINA5* and could be distinguished
135   as a satellite glial cell (SGC) population, while the lack of *SERPINA5* allowed the labeling of
136   clusters 1 and 8 as non-myelinating Schwann cells. Cluster 2 and cluster 12 both showed
137   unique distinct expression of *VWF/EGFL7* and *NOTCH3/MYH11* indicating endothelial and
138   mural cell populations, respectively.

139       Twelve neuronal clusters were characterized as shown in the UMAP in Figure 1G.
140   Based on marker gene expression clusters 1, 5, 8 and 9 were identified as non-nociceptive
141   (*NTRK2*/*NTRK3*) and clusters 0, 2, 3, 4, 6, 7, 10 and 11 as likely nociceptors
142   (*SCN10A/TRPA1/SST)*), based on marker gene expression (Fig 1H). Additionally, cluster 2
143   could be identified as TRPA1+ nociceptors, and cluster 10 and 11 expressed *CHRNA3, SST,*
144   *NNPB* and *OSMR* indicating putative silent nociceptor populations. Other marker genes,
145   including *PENK* and *TRPM8* expressions, did not appear highly expressed. We, consequently,
146   sought to use additional approaches to characterize the neuronal subtypes in greater detail.

147   ***Comparison of C2 DRG neurons to thoracic and lumbar DRG and TG populations***

148    To characterize the neuronal clusters of the C2 DRG, we utilized previously published
149    labeling of human DRG, as well as trigeminal ganglia (TG) (Tavares-Ferreira et al., 2022;
150    Bhuiyan et al., 2024). Using CONOS (Barkas et al., 2019), we transferred labels from neurons
151    characterized in lumbar DRGs onto the C2 DRG data (Fig 2A). The UMAP, which shows a
152    spatial representation of transcriptional similarity between nuclei, showed the groupings
153    identified in C2 DRGs correlating with labels from lumbar DRGs. In Figure 1B, violin plots
154    showed the proportions of clusters from lumbar DRGs identified in each of the C2 clusters.
155    Cluster 1 contained A-beta LTMR and A-delta LTMR neurons. Cluster 2 contained primarily
156    TRPA1+ nociceptors, as well as minor proportions of PENK+ and cold nociceptors. Cluster 10
157    was unique in distinctly correlating with the labeling of putative silent nociceptors. Interestingly,
158    cluster 7 was found to contain transcriptional similarity to all neuronal subtypes identified in
159    lumbar DRG, while exhibiting a very low number of enriched genes, indicating high
160    transcriptional heterogeneity in the cluster. Enriched expression of *PKD1* and *PDIA2*, two genes
161    that have previously been associated with injured neurons in the study of Parkinson's disease,
162    was observed in cluster 4, 6, 8, 9 and 11 which surrounded cluster 7 in Figure 1H (Conn et al.,
163    2004; Amadesi et al., 2009; Asaithambi et al., 2011). The probability of transcriptional similarity
164    between clusters 4, 7, 8 and 9 is high, based on the proximal location of nuclei in the UMAP. In
165    fact, the UMAP in Figure 2A with label transfer revealed the clusters in the lower right quadrant
166    appeared to include smaller subsets of all neuronal subtypes, and these clusters all, apart from
167    7, showed *PKD1* and *PDIA2* enrichment (Supplementary table 1A). Importantly, the source
168    material for this study was patient surgeries, specifically patients receiving surgery for either
169    acute traumatic injury or chronic ongoing degeneration of the joint. Consequently, injured
170    neurons may have originated from the ongoing disease state whether it was chronic neck pain
171    with arthritis or acute neck injury requiring C1-2 fusion. Interestingly, these genes are detected
172    in previous studies of hDRG but are lowly expressed in mouse (Jung et al., 2023; Bhuiyan et al.,
173    2024), and are not known to be changes by injury in the mouse DRG (Renthal et al., 2020),
174    suggesting that these genes could be markers of neuronal injury in C2 hDRG.

175    We additionally used DRG and TG neuron labels characterized using single-nuc
176    RNAseq in the harmonized atlas by Bhuiyan et al. to assess the similarity to C2 DRG neurons to
177    lumbar and thoracic DRG neurons and TG neurons (Fig 2C-E). *PVALB+* and *DCN+* neuronal
178    populations labeled in lumbar and thoracic DRGs were observed in clusters 5, 7 and 9 in C2
179    DRGs (Fig 2C-D). *ASIC1* was enriched in clusters 5 and 9 indicating non-nociceptive neurons.
180    Neuronal populations identified in TG defined by *Mrgpra3+* (orthologous to human *MRGPRX*
181    genes) were observed in C2 DRGs, in clusters 2, 3, 4, 5, 7, 8 and 10 (Fig 2E). Additionally,
182    *MRGPRX1* was found to be enriched in clusters 3 and 8 (Fig 2F). *MRGPRX1+* neurons were
183    exclusively identified in TG in human samples in the harmonized atlas (Bhuiyan et al., 2024),
184    however, it was hypothesized that they were a rare cell type in the DRG (Yu et al., 2024). The
185    enrichment of *MRGPRX1+* neurons may indicate a higher proportion of this cell-type in cervical
186    DRGs, similar to TG (Tavares-Ferreira et al., 2022; Bhuiyan et al., 2024). *TRPM8*, which has
187    previously been shown to be enriched in TG compared to DRG in rodents (Kobayashi et al.,
188    2005), was lowly expressed in C2 DRG, and not enriched in any cluster. *CALCA*, while being
189    expressed in both DRG and TG, has been described as highly expressed in TG and
190    characterized as playing a role in migraine (Goadsby et al., 1990; Ohlsson et al., 2018). *CALCA*
191    was identified as enriched in 4 neuronal clusters (0, 2, 4, 10), correlating with nociceptive
192    clusters.

193       In mice, characterization of TG in comparison to DRG has revealed distinct
194    transcriptomic patterns. In a study by Megat et al., 381 DEGs were identified as highly enriched
195    in TG. When comparing the genes identified as enriched in TG and DRG in mice and
196    overlapping with enriched genes in each of the C2 clusters, clusters 0, 1, 5, 8 and 9 all had a
197    higher number of enriched genes in the TG (Supplementary table 1B). *Fth1* and *Pak1* were
198    identified as highly enriched in TG. Both of these genes have human orthologues, *FTH1* and
199    *PAK1* (Megat et al., 2019a). *PAK1* was observed to be enriched in clusters 1 and 5 (A-fiber
200    LTMRs and proprioceptors when labeled according to DRG nomenclature) (Fig 2G). *FTH1* was
201    expressed in multiple clusters and not enriched in one specific cluster (Fig 2H). Interestingly, in
202    human lumbar DRGs characterized with spatial sequencing, *FTH1* was observed as broadly
203    expressed in all neuron populations, while *PAK1* was very lowly expressed (Tavares-Ferreira et
204    al., 2022), indicating both species and DRG-level differences in the C2 DRG.

205       Hematoxylin and eosin (H&E) stained sections of 4 C2 DRGs were used to measure the
206    average neuronal cell size (Fig 2I). The range of diameter of 407 neurons was 30 to 100 μm.
207    This range falls in between the size-ranges reported for neurons in the lumbar DRGs in humans
208    (30-125 μm) (Tavares-Ferreira et al., 2022) and trigeminal neurons (30-80 μm) (Shiers et al.,
209    2023). The mean neuron diameter of C2 DRG neurons was 64 μm, which aligned closely to the
210    lumbar DRG mean of 67 μm, while TG neurons were 41 μm.

211       In summary, we observed that the neuronal cells in C2 DRGs exhibit similarities to both
212    lumbar DRGs and TG. All neuronal subclusters characterized in lumbar DRGs were identified in
213    C2 DRG, however, physical characterization of C2 DRGs reflected a reduction in size range
214    compared to lumbar DRGs. This finding correlated with the clusters shown to exhibit
215    transcriptional similarities to TGs: Clusters 0, 1 and 5, labeled as A-fiber LTMRs with label
216    transfer and consequently most closely aligned transcriptionally to larger neurons. These A-fiber
217    LTMR clusters also exhibited enrichment of genes characterizing the TG, including *PAK1.*
218    Additionally, clusters 3 and 8, identified as likely pruritogen receptor enriched neurons, are
219    enriched for *MRGPRX1*, a gene showing robust expression in TG and minimal expression in
220    lumbar DRGs.

221    ***Transcriptomic differences between C2 DRGs recovered for acute injury or chronic pain***
222    ***reflect results from transcriptomic/genomic wide association studies***

223       The cervical DRGs were recovered during surgery from patients suffering either acute
224    trauma or long-term osteoarthritis of the joint associated with chronic pain. Based on
225    quantitative sensory testing (QST) and analysis of self-reported pain scores from patients prior
226    to surgery, it is apparent that the chronic pain experience in most of these patients does not
227    match characteristics that would classify the pain of these individuals as having neuropathic
228    pain (Table 1 and 2). Most individuals did not demonstrate signs of mechanical allodynia, and
229    only a small number of patients in the chronic pain group showed signs of cold hypersensitivity.
230    The major difference in terms of QST and pain report measures was the duration of pain, which
231    was much greater in the chronic pain group. This provided a unique opportunity to assess the
232    molecular differences driving chronic neck pain, in a well-characterized subgroup of patients.
233    We analyzed neuronal clusters and non-neuronal clusters, the latter of which were
234    amalgamated into 7 distinct clusters based on marker gene enrichment as described above
235    (Supplementary table 1C), to identify transcriptomic differences in these cell types associated
236    with chronic pain (Fig 3A-B). Differential gene expression was measured with DESeq2 and
237    defined as genes with adj. p-value < 0.05 and $|Log_2FC| > 0.5$.

238  No differential genes were identified in any neuronal cluster; however, differential
239  expression patterns were discovered in endothelial, fibroblast and myelinating Schwann cells
240  (Fig 3C-E). In the endothelial cluster, 121 genes were identified, 114 of which were upregulated
241  in samples with chronic pain (Fig 3C, Supplementary table 2A). Upregulated genes included
242  *C8orf34*, *ICOS*, *CD2*, *FKBP5,* and *CXCL2*. *C8orf34* has previously been associated with chronic
243  back pain in multiple GWAS (Freidin et al., 2019; Li et al., 2023; Belonogova et al., 2025).
244  Upregulation of *CXCL2,* a pro-inflammatory chemokine ligand, has been associated with
245  neuropathic pain and orofacial trigeminal pain (Iwasa et al., 2019; Solis-Castro et al., 2021;
246  Hummig et al., 2023; Zeng et al., 2023). Blockage of *FKBP5*, FK506-binding protein 5, has
247  previously been shown to relieve inflammatory pain states in mice (Maiarù et al., 2018). *CD2* is
248  an adhesion molecule usually observed on the surface of T-cells, and associated with an
249  inflammatory state driven by active T-cells. In contrast, *ICOS* has been suggested to alleviate
250  mechanical hypersensitivity induced by paclitaxel through T-cell activation (Sankaranarayanan
251  et al., 2023a). T-cell activity has previously been attributed to both pro- and anti-nociceptive
252  roles depending on the pathway of activation (Ji et al., 2016). Pathway analysis of the DEGs
253  showed enriched Th1 and Th2 cell differentiation as well as IL-17 signaling, implicating
254  endothelial cells in inflammation in chronic pain through interactions with immune cells.

255  Twenty-five genes were found to be upregulated in fibroblast cells (Fig 3D,
256  Supplementary table 2B). *C8orf34*, *FGFBP2* and *CCN3* were among upregulated genes.
257  *C8orf34* does not have a known function, but was also upregulated in endothelial cells
258  suggesting that it may play a generalized role in non-neuronal cells in arthritic neck pain.
259  *FGFBP2*, which encodes fibroblast growth factor binding protein 2, has been associated with
260  Modic changes in intervertebral disc degeneration and has been implicated as a possible blood
261  biomarker of chronic neuropathic pain (Cherif et al., 2022; Islam et al., 2022; Rajasekaran et al.,
262  2022). *CCN3* was identified as the most highly enriched gene in fibroblasts, and this gene has
263  been identified as playing a key role in the pathology of rheumatoid arthritis through
264  inflammatory fibroblasts (Tokuhiro et al., 2024).

265  In myelinating Schwann cells, 55 genes were found to be differentially expressed, 33 of
266  which were upregulated in chronic pain (Fig 3E, Supplementary table 2C). *FGFBP2* was
267  upregulated in both fibroblasts and myelinating Schwann cells, again suggesting a generalized
268  role for this gene in arthritic neck pain. *FKBP1*, involved in the stress response and
269  inflammatory pain was upregulated in both Schwann cells and endothelial cells (Maiarù et al.,
270  2018). Furthermore, *MKNK2*, which encodes the mitogen activated protein kinase interacting
271  kinase (MNK) 2, was upregulated. MNK2, is a key mediator of inflammation through translation
272  mediation, and has previously been associated with inflammatory dysregulation driving pain
273  (Moy et al., 2017; Moy et al., 2018). *METRN* and *NRG1* were also identified as differentially
274  expressed. *METRN,* which encodes a secreted protein without a known receptor, was
275  upregulated in chronic pain. Interestingly, previous research suggests a role for *METRN* in
276  resolving neuropathic pain (Jørgensen et al., 2012; Sankaranarayanan et al., 2025). *NRG1*,
277  which encodes neuregulin-1, was upregulated in acute pain. Neuregulin-1 is ascribed a
278  neuroprotective role through immunoregulation driven by the NF-kB pathway (Simmons et al.,
279  2016), however, it has also been indicated to drive neuropathic pain states through
280  phosphorylation of ERK1/2 (Calvo et al., 2011; Dai et al., 2014).

281  In summary, snRNAseq of C2 DRGs showed the primary transcriptional difference was
282  manifesting in non-neuronal cells. The differentially expressed genes in the endothelial cells,

283     fibroblasts and Schwann cells reflect abnormal transcriptional patterns indicating activation of
284     inflammatory pathways. Simultaneously, multiple transcripts, including *METRN* in Schwann cells
285     and *ICOS* in the endothelial cluster, indicate activation of neuroprotective mechanisms
286     potentially preventing the development of a neuropathic pain state. To assess whether the
287     transcriptional patterns reflected changes to the physical architecture of the DRG we used
288     additional RNA sequencing approaches.

289     ***Inflammatory transcriptomic patterns observed in chronic pain C2 tissues with***
290     ***multiple sequencing approaches***

291     Bulk RNAseq was carried out on 17 DRGs from 13 patients to assess transcriptomic
292     changes in the whole C2 DRG when comparing acute and chronic pain. Fourty DEGs were
293     identified, 17 of which were upregulated and 23 downregulated in chronic pain (Fig 4A,
294     Supplementary table 3A). One gene correlated with findings from snRNAseq, specifically
295     decreased expression of *SLCO2A1*, a transporter of prostaglandin (Fig 4B). The transporter
296     plays a role in clearing prostaglandin E2, $PGE_2$, a key mediator of inflammatory pain (Davies et
297     al., 1984; Nakanishi et al., 2021). Additionally, *SLCO2A1* mutations are causative of
298     hypertrophic osteoarthropathy, a disease characterized by inflammation in bones and joints (Lu
299     et al., 2023). Decreased expression of the $PGE_2$ transporter suggests a disruption in $PGE_2$
300     metabolism, with the upregulation of $PGE_2$ in the C2 DRG contributing to inflammatory
301     dysregulation. Consequently, multiple transcriptional changes are observed in the C2 DRG with
302     bulk RNAseq and snRNAseq which reflect inflammatory pathways that may contribute to
303     abnormal pain signaling. Several genes are observed in more than one cell-type with snRNAseq
304     or in multiple sequencing approaches (Fig 4B-C). To assess the spatial organization of these
305     changes in gene expression, we employed spatial RNAseq.

306     We obtained spatial transcriptomic data from 13 C2 DRGs from 8 patients. Sections of
307     DRG were sectioned onto Visium slides with 55 µm barcoded spots and imaged following H&E
308     staining to obtain spatial information. Unique barcodes corresponding to spatial location were
309     bound to mRNA in each section to obtain spatially correlated transcriptomic data. We visually
310     confirmed barcodes that overlapped neurons and defined barcodes as (1) neuronal, (2)
311     immediately surrounding a neuron (surrounding), and (3) others, as defined previously (Tavares-
312     Ferreira et al., 2022). No differentially expressed genes were identified when comparing
313     samples from acute and chronic patients in any group of barcodes. This may be due to
314     insufficient sample size to find differences using this technique. However, the Visium data
315     allowed for a spatial characterization of the DEGs from bulk- and snRNAseq. The expression of
316     *SNAP25* was primarily observed in neuronal barcodes, validating the barcode groups (Fig 4D).
317     *SNAP25* consequently visualizes the neurons in samples 26 (chronic pain) and 27 (acute pain)
318     in Figure 4E-F. Subsequently, we evaluated the spatial expression patterns of *FGFBP2*, *METRN*
319     and *SLCO2A1*. *FGFBP2* was upregulated in chronic pain in myelinating Schwann cells and
320     fibroblast cells, while *METRN* was upregulated in Schwann cells. Using the spatial
321     transcriptomics data, *FGFBP2* and *METRN* expression in sample 26 appears similar, visually
322     localizing near the areas with *SNAP25* expression. The remaining *SLCO2A1*+ barcodes were
323     also proximal to *SNAP25*+ areas. However, when considering all samples, *METRN* was
324     primarily measured within neuronal barcodes, while *FGFBP2* was measured in Other barcodes
325     (Fig 4). In contrast, the expression of *SLCO2A1*, which was downregulated in chronic pain with
326     bulk RNAseq and snRNAseq, was absent in neuronal barcodes. The expected consequence of

327  this downregulation would be increased PGE$_2$ concentration in the area around C2 DRG
328  neurons.

### Predicted communication between neuronal and non-neuronal cells driving chronic pain states

331  The transcriptional changes in the chronic pain C2 DRG indicate a reorganization of the
332  transcriptomes of certain non-neuronal cell types with little change in the neuronal populations.
333  In order to assess how the non-neuronal cells may exert an impact on neuronal cells, we used
334  interactome analysis. We assessed ligand genes that were upregulated in non-neuronal cell
335  types in chronic pain C2 DRGs and intersected these genes with receptors for these ligands
336  that are expressed by different populations of C2 DRG neurons. This analysis showed
337  interactions between non-neuronal (endothelial, fibroblast and myelinating Schwann cells) and
338  neuronal cells corresponding to a curated database of ligand-receptor interactions (Fig 5A-C).
339  *EDN1* and *EFNA1* were identified as expressed in endothelial cells with multiple receptors and
340  interactions in neurons: *EFNA1*, which encodes an ephrin protein, interacted with tyrosine
341  kinase receptors encoded by *EPHA* and *EPHB* genes (Fig 5A-B). *EPHA3/5* showed higher
342  expression in nociceptor cells, indicating a more likely interaction with nociceptors, while the
343  remaining *EPHA* genes were more highly expressed in non-nociceptive neuronal clusters (Fig
344  5C). *EDN1* interacts with *EDNRA*, *KEL* and *ADGRL4*. *EDN1* interaction with the receptor
345  *EDNRA* is likely the most important in this context as a genome association also study found
346  correlation between *EDNRA* and migraine (Lisi et al., 2006; Miao et al., 2012), previous studies
347  have shown that endothelin 1 causes pain like behavior in rodents through the *EDNRA* receptor
348  (Zhou et al., 2001; Zhou et al., 2002), and the *EDN1-EDNRA/EDNRB* axis has been linked to
349  oral cancer pain (Zhou et al., 2002; Dang et al., 2020). *CSF3* and *IL34* were upregulated in
350  chronic pain in endothelial cells, and found to interact with *CSF1R* and *CSF3R*, both of which
351  showed higher expression in nociceptor subtypes (Fig 5B-C). *IL34* encodes a cytokine that
352  interacts with *CSF1R*, which has previously been associated with inflammation, as well as
353  several pain conditions including bone pain, arthritis, and neuropathic pain (Schweizerhof et al.,
354  2009; Bali et al., 2013; Guan et al., 2016; Ushach and Zlotnik, 2016; Lee et al., 2017; Lin et al.,
355  2019) Additionally, *CXCL2*, a chemokine characterized in neuropathic pain, and specifically in
356  trigeminal pain, was found to interact with three chemokine receptors in neurons (Iwasa et al.,
357  2019; Solis-Castro et al., 2021; Hummig et al., 2023; Zeng et al., 2023).

358  Fewer differentially expressed genes were identified in myelinating Schwann cells and
359  fibroblasts, consequently the identified interactions with neurons were limited (Fig 5A-B). *CCN3*,
360  which was upregulated in fibroblasts and previously characterized in arthritis (Tokuhiro et al.,
361  2024), was indicated to interact with *PLXNA1*, which was broadly expressed in neurons (Fig 5A-
362  C). *CADM4* is a cell adhesion molecule, the interactions of which exhibited a trend towards
363  increases in nociceptors (Fig 5C). *CADM4* activity with *ERBB3* and *PTPN13* has primarily been
364  characterized in relation to myelin formation, and an increase in CADM4 expression has been
365  associated with abnormal myelination formation (Elazar et al., 2019). *CADM4* additionally
366  interacts with *KDR*, which encodes the receptor VEGFR2. VEGFR2 has been associated with
367  synapse formation and neuronal guidance (De Rossi et al., 2016). The dysregulation of CADM4
368  could consequently be theorized to impact innervation.

369  Altogether, a transcriptome pattern reflecting the upregulation of regulators of
370  inflammation, mediated by non-neuronal cells, is observed in C2 DRGs from patients with
371  chronic pain. The transcription patterns are reflected both in the proximal area of neurons as

9

372    well as in distant areas, suggesting widespread dysregulation across neuronal and non-
373    neuronal networks.

374    **Discussion**

375         Our work on C2 DRGs recovered from patients undergoing arthrodesis surgery with
376    ganglionectomy led to the following major conclusion. First, consistent with the innervation
377    patterns for C2 DRGs that share properties with lumbar DRGs and TGs, we found that these
378    neurons represent a mixed transcriptomic phenotype between DRG and TG neurons. Second,
379    we found that most transcriptomic changes in chronic pain C2 DRGs were associated with non-
380    neuronal cells including endothelial, myelinating Schwann cells, and fibroblasts. These changes
381    were mostly associated with inflammation and suggest that arthritis of the atlantoaxial joint in
382    humans causes inflammatory-related changes in gene expression in the associated C2 DRG.
383    Finally, integrating our single nucleus sequencing results with spatial transcriptomic data and a
384    ligand-receptor interaction database revealed potential mechanisms that might be pain
385    generators within the C2 DRG in individuals with chronic neck pain. These mechanisms
386    included signaling molecules like endothelin-1 (Zhou et al., 2001; Zhou et al., 2002), FKBP5
387    (Linnstaedt et al., 2018; Geranton, 2019; Maiaru et al., 2023; Ahlstrom et al., 2024; Lafta et al.,
388    2024), and MNK2 (Moy et al., 2017; Moy et al., 2018; Megat et al., 2019b; Shiers et al., 2023;
389    David et al., 2024; Li et al., 2024; Mitchell et al., 2024)  that have previously been associated
390    with pain in animal models and human studies, and mechanisms that might promote neuronal
391    sprouting which could cause pathological changes in innervation in chronic neck pain.

392         The human C2 DRG appears to share properties of more caudal DRGs and the TG. The
393    C2 DRG is unique because it innervates areas of the upper neck but also contain neurons that
394    innervate the occipital dura, a specialized tissue protecting the brain that is also innervated by
395    the TG and implicated in migraine and other headache disorders (Keller et al., 1985; Noseda et
396    al., 2019). This anatomical connection is one of the explanation why painful lesions of the upper
397    cervical spine can be associated with headache. (Bogduk and Govind, 2009). We found several
398    genes that were highly expressed in the C2 DRG that are also enriched in the TG, such as
399    *FTH1* and *PAK1* which were identified in a study in mice (Megat et al., 2019a), and MRGPRX1
400    which was identified in humans as enriched in the TG (Bhuiyan et al., 2024). While many
401    different atlases of hDRG neurons have been published to-date (Nguyen et al., 2021; Tavares-
402    Ferreira et al., 2022; Jung et al., 2023; Bhuiyan et al., 2024; Yu et al., 2024), none of them have
403    focused on understanding variation in gene expression based on the level of the DRG. Our work
404    shows that the C2 DRG has some unique transcriptomic features and makes the case that
405    future work should strive to better understand molecular features of human sensory neurons
406    along the entire caudal to rostral extent of the peripheral nervous system from sacral DRGs to
407    the TG.

408         We did not find evidence of neuropathic pain in our chronic neck pain cohort in
409    somatosensory measures, except cold allodynia in 2 patients (Table 2), or in the transcriptome
410    of the C2 DRGs of these individuals. Neck pain is considered of primary musculoskeletal nature,
411    but neuropathic components are possible. The C2 DRG is located between the arch of C1 and
412    the lamina of C2. In this space, the DRG occupies 76% of the foramen height, rendering the
413    ganglion vulnerable to compression in patients with altered spine due to arthritis or fractures (Lu
414    and Ebraheim, 1998). Recent studies of patients with whiplash injury suggest that there is a
415    prominent neuropathic phenotype in these patients with loss of sensory function, mechanical
416    and cold hypersensitivity, neuroinflammation evident with imaging, and increased measures of

417  neurofilaments in plasma, consistent with neuronal injury (Fundaun et al., 2025; Ridehalgh et
418  al., 2025). Table 2 shows some more neuropathic pain characteristics in the acute pain cohort,
419  which may be closer to the whiplash injury phenotype.

420      In DRGs from chronic pain patients in our study, we noted some changes in the neuronal
421  transcriptome that could be associated with neuronal injury (in both the acute and chronic
422  cohort) that were characterized by neurons expressing *PKD1* and *PDIA2*. These neurons mostly
423  had similar transcriptomes to matching populations within the C2 DRG not expressing these
424  genes, and did not undergo wholesale changes in their transcriptomes as has been reported in
425  animal models of nerve injury (Renthal et al., 2020). To our knowledge, *PKD1* and *PDIA2* have
426  not previously been reported as markers of nerve injury in the DRG, but they have been
427  associated with nerve injury in Parkinsons disease (Conn et al., 2004; Amadesi et al., 2009;
428  Asaithambi et al., 2011). A question that emerges from these findings is that if there is evidence
429  of nerve injury, and neuropathic pain is common among people with chronic neck pain, why do
430  individuals in this cohort fail to develop signs of neuropathic pain? One possibility is that
431  mechanisms that suppress neuropathic pain are also induced in the DRG of these individuals.
432  For instance, we observed increased *ICOS* and *METRN* expression in single nuc RNA
433  sequencing data in patients in the chronic pain cohort. Previous work suggests that *ICOS*
434  stimulates T-cells to produce interleukin-10 to suppress neuropathic pain (Sankaranarayanan et
435  al., 2023a). Several studies have shown that meteorin, the protein encoded by the *METRN*
436  gene, can reverse established neuropathic pain states in both mice and rats (Jorgensen et al.,
437  2012; Xie et al., 2019; Sankaranarayanan et al., 2023b). While this idea clearly requires further
438  exploration, it is interesting that pain promoting and pain-resolution mechanisms seem to be
439  induced at the same time in the DRGs of the individuals with chronic neck pain studied here.
440  Another explanation for the limited evidence for neuropathic components is our limited ability to
441  detect painful neuropathy, which relies mostly on somatosensory measures at the skin that may
442  not capture painful neural lesions of deep tissues.

443      Our study identifies potential mechanisms of chronic neck pain that can be targeted by
444  therapeutics. These include *FKBP5*, endothelin-1 and the endothelin A receptor, MNK2
445  signaling, and *IL34* acting via the *CSF1* receptor. All of these signaling factors have previously
446  been implicated in pain, but none of them have been associated with neck pain, to our
447  knowledge. This is not surprising because there are few animal models of neck pain and the
448  disorder, while both prevalent and disabling in the human population, is challenging to study at
449  the molecular level. Therefore, an important strength of this study is the molecular insight our
450  work might give to developing new targets for the treatment of neck pain. *FKBP5* encodes the
451  FKBP51 protein that is involved in glucocorticoid signaling. The protein has been implicated in
452  the important link between stress and pain and could be targeted with inhibitors of the protein
453  (Linnstaedt et al., 2018; Geranton, 2019; Maiaru et al., 2023). We identified increased
454  endothelin-1 gene expression in endothelial cells of the chronic pain cohort. The receptor for
455  this protein, the endothelin A receptor, is highly expressed in rodent and human nociceptors and
456  activating the receptor causes pain in rodents through signaling cascades that involve voltage
457  gated sodium channels (Zhou et al., 2001; Zhou et al., 2002; Bhuiyan et al., 2024). *MNK2*
458  encodes a mitogen activated protein kinase (MKNK2) that has been implicated in pain through
459  mouse genetic studies and studies on hDRG neurons. Inhibiting MNK with the specific inhibitor
460  eFT508 leads to decreased pain in mouse studies and a reduction in excitability in human
461  nociceptors (Moy et al., 2017; Megat et al., 2019b; Li et al., 2024). IL34 was upregulated in
462  endothelial cells in the DRG of chronic pain patients in this cohort. The receptor for this

11

463     cytokine, CSF1R is strongly expressed across neuronal populations in the human C2 DRG but
464     the consequences of activation of CSF1R in hDRG have not yet been studied. We propose that
465     these targets should be prioritized for future investigation as therapeutic interventions for non-
466     neuropathic chronic neck pain.

### *Limitations*

468     This study was designed to identify changes in a unique subpopulation of patients, by
469     utilizing an opportunity to recover tissues otherwise discarded during surgery. However, as the
470     primary source was surgical tissue, we did not have access to control samples from a patient
471     population without pain. The physical location of the cervical DRGs in the upper neck makes it
472     challenging to access them during a standard organ donor tissue recovery without an additional
473     incision that can interfere with subsequent tissue recovery for tissue donation. Since recovery of
474     DRGs following organ donation has become an important source of these tissues for research
475     purposes (Shiers et al., 2024), this issue will need to be overcome to obtain control samples of
476     C2 DRGs.

477     Another limitation is the small sample size in this study. C1-2 arthrodesis is an
478     uncommon procedures, and resection of the DRG as part of clinical care is not uniform practice
479     among surgeons. Given the difficulty in obtaining these samples, and the lack of information on
480     C2 DRG in humans we think that the insight provided from this study justifies the small sample
481     size. Previous work on thoracic DRGs recovered during thoracic vertebrectomy surgery
482     demonstrated that findings from an initial, smaller cohort, were replicated in a larger cohort
483     collected over a longer period of time (North et al., 2019; Ray et al., 2023). We plan to use a
484     similar approach as this unique cohort of patients continues to grow.

485

### **Materials and methods**

### *Study design*

488     The goal of this study was to characterize human C2 DRGs with molecular precision. For this
489     purpose, DRGs were collected from patients during C1-C2 arthrodesis surgery with
490     ganglionectomy for acute or chronic pain. All human tissue procurement protocols were
491     reviewed and approved by the University of Texas at Dallas (UTD) and University of Washington
492     (UW) Institutional Review Boards. Patient information, including demographics and
493     characterization of clinical presentation, was collected from medical records and self-reported
494     questionnaires prior to surgery.

### *Participants and setting*

496     Patients eighteen years or older undergoing C1-C2 arthrodesis for neck pain at the University of
497     Washington were prospectively recruited. The study was reviewed and approved by the
498     University of Washington Internal Review Board (IRB number 10916). Informed consent was
499     obtained from all patients, who were offered a $125 gift card for participating in the study.

500     Patients were identified from emergency care settings and clinic visits. We screened for patients
501     who were greater than eighteen years old, undergoing C1-C2 arthrodesis. These patients were
502     identified in a two-pronged manner, whereby the surgeon would notify the research staff of
503     scheduled procedures, and by daily electronic reports accessing the feeds of surgery

504    scheduling data, using the UW Medicine Enterprise Data Warehouse. Exclusion criteria were
505    cognitive deficits or language comprehension that would make the patient unable to consent.
506    Potentially eligible outpatients were contacted via phone call to set up a time to meet in person
507    and inpatients were met in their hospital room if they indicated interest in potentially participating
508    in the study. The research staff then informed the participant of the study and consent the
509    patients using a standardized consenting script.

510    Participants were categorized as having acute (lasting <3 months) and chronic pain (≥3
511    months), in keeping with the definitions of the International Association for the Study of Pain
512    (IASP) (Treede et al., 2019).

### *Sociodemographic variables and patient-reported outcomes*

514    Age, sex, body-mass index (BMI), opioid medication, race, and ethnicity were recorded within
515    two weeks of the surgery from the electronic health records (EHR) when available, or were
516    otherwise confirmed by patient interview.

517    Measures of pain included location of pain, duration of pain (days), average pain in the last 24
518    hours on the most painful side of the neck, and neck-related function. Patients were asked to
519    rate their average neck/occipital pain during the last 24 hours on their most painful side using
520    the numerical rating score (NRS), with 0 = no pain and 10 = worst pain imaginable (Dworkin et
521    al., 2005). Patients were asked to indicate the duration of their pain, which was recorded in
522    days. Neck-related function was assessed using the 5-item version of the Neck Disability Index
523    (NDI-5) (Walton and MacDermid, 2013).

### *Somatosensory measures*

525    Patients underwent quantitative sensory tests (QST) according to published guidelines (Cruccu
526    et al., 2010) using a standardized and widely used protocol (Backonja et al., 2013). The QST
527    was performed on the most painful side of the neck (or randomly selected side in case of equal
528    bilateral pain). The instruments involved include a soft brush to simulate light brushing, a
529    monofilament to simulate light pressure, and a tuning fork that has been in ice water to simulate
530    coolness. Patients were asked to rate the sensation of brushing, pressure, and coolness from a
531    0 = felt nothing to 10 = extremely intense feeling, and secondarily whether any of the three
532    modalities cause pain.

533    Temporal summation, the increased perception of pain in response to sequential stimuli of equal
534    physical strength, was used as an indicator of facilitated pain modulation processes at the neck
535    (Price, 1972; Arendt-Nielsen et al., 1994; Staud et al., 2007). A pinprick stimulator was used to
536    measure the intensity of a single point of stimulus using a 0-100 NRS (0 = no pain, 100 = worst
537    pain imaginable). Ten additional stimuli were subsequently administered, and patients were
538    asked to rate that sensation using the same scale. The temporal summation effect was
539    calculated by subtracting the pain intensity after 10 stimuli by the pain intensity after one
540    stimulus.

541    Pressure pain sensitivity was conducted using a pressure simulation device (Wagner FDK 40).
542    Gradually increasing pressure at the rate of (0.5 kg-force/s) was administered, and the
543    participant was instructed to inform the researcher of the moment that the sensation changes
544    from a feeling of pressure to a feeling of pain by voice (e.g., 'stop', 'now,'). The recorded
545    pressure (kg) was defined as pressure pain threshold.

13

### Tissue collection

546 DRGs were collected from 11 patients with chronic pain and 11 patients with acute pain
547 according to previously described protocol(Hofstetter, 2025). Briefly, C1 lateral mass screws
548 were placed at the midpoint C1 posterior arch and the lateral mass, and C2 pars screws were
549 placed at a parallel trajectory to the C2 pars to ensure fixation. A bilateral C2 DRG neurectomy
550 was performed and DRGs were immediately placed in powdered dry ice to ensure uniform
551 freezing to preserve RNA. DRGs were shipped to UTD for all sequencing experiments.

### Single-nucleus RNA sequencing

554 To achieve characterization at a molecular level, we used 10X single-cell RNA-sequencing of 12
555 DRGs from 12 patients. Briefly, DRGs were thawed in artificial cerebrospinal fluid (aCSF) and
556 perineurium as well as cauterized exterior tissue was removed to expose clean C2 DRG bulb.
557 The bulb was dissociated and filtered to minimize myelin contamination and obtain individual
558 nuclei according to previously published 10X protocol (Lacagnina et al., 2024). The RNA from
559 each nucleus was barcoded and libraries were generated according to the manufacturer's
560 protocol for sequencing on a NextSeq2000 at the genomic core at the University of Texas Dallas
561 or Psomogen.

### Spatial RNA sequencing

563 We used 10X Visium spatial transcriptomics to achieve near-single resolution data, retaining
564 concurrent transcriptional and spatial information, according to previously published protocol
565 (Tavares-Ferreira et al., 2022). Briefly, 13 DRGs from 8 donors were sectioned onto Visium
566 slides, stained with hematoxylin and eosin (H&E) and imaged. Tissue permeabilization and
567 binding of oligo primers were performed according to the manufacturer's instructions.
568 Sequencing of mRNA libraries was performed on a NextSeq2000 at the genomic core at the
569 University of Texas Dallas and barcodes overlapping neurons were identified visually and
570 confirmed through expression of neuronal marker *SNAP25*.

### Bulk RNA sequencing

572 To assess transcriptomic differences to the whole DRG associated with pain phenotype, we
573 used bulk RNA sequencing. Briefly, RNA was extracted from 23 C2 DRGs from 13 donors.
574 Three 100μm sections from the bulb were lyzed in TRIZol and RNA extracted with chloroform.
575 DNA was depleted using Qiagen DNase I, according to manufacturer's instructions. RNA
576 integrity was assessed with nanodrop and Qubit and samples with RNA integrity number 2.4-8.1
577 were sequenced using NextSeq2000 for paired-end mRNA sequencing. Five samples were
578 excluded due to low gene expression of neuronal markers according to a previous analysis (Ray
579 et al., 2023), thus 17 DRGs from 13 donors were included in downstream analysis.

### Computational analysis

*Single-nucleus RNA sequencing Pipeline*

582 Sequencing data were processed and mapped to GRCh38 human reference genome
583 (GENCODE release 38) according to 10X protocol using package cellranger. Nuclei with less
584 than 500 genes or more than 7.5% mtRNA were excluded from downstream analysis. Unbiased
585 clustering was performed using the Seurat package v5.2.1. Neuronal and non-neuronal clusters
586 were identified through marker gene enrichment of neuronal markers (*SNAP25*, *RBFOX3* and

587   *PRPH*) and non-neuronal markers (*SPARC, MPZ* and *DCN*). FindAllMarkers was used to
588   identify gene enrichment (|Log$_2$FC>0.5|, adj. p-value<0.05 and min. percent expression in 25%
589   of cluster). The neuronal and non-neuronal clusters were subset into separate objects for
590   downstream analysis. Counts were aggregated for cells of the same cluster for each donor, for
591   differential gene expression analysis with DESeq2 (Love et al., 2014). Differential gene
592   expression analysis was carried out to account for batch effects and sex differences: design = ~
593   Sex + Batch + Condition. Differentially expressed genes (DEGs) were defined as |Log$_2$FC>0.5|,
594   adj. p-value<0.05.

595   *Bulk RNA sequencing Pipeline*

596   Raw sequencing (FASTQ) files were processed with FastQC v0.11.0 to examine Phred scores,
597   per-base sequence, and duplication levels. Reads were soft-clipped (12 bases per read) to
598   discard adapters and low-quality bases during alignment using STAR v2.7.6 (Dobin and
599   Gingeras, 2015) with the GRCh38 human reference genome (GENCODE release 38, primary
600   assembly). Reads were also sorted with STAR and then deduplicated with sambamba v0.8.2
601   (Tarasov et al., 2015). Genes in the ENCODE blacklist were filtered out prior to quantification
602   using bedtools (v2.30.0), and StringTie v2.2.1 was used to obtain normalized count values as
603   transcripts per million (TPM) for each gene of all samples (Quinlan, 2014; Pertea et al., 2016;
604   Amemiya et al., 2019). The featureCounts function of the R package Rsubread (v2.14.2) was
605   used to calculate raw counts for all genes, which was subsequently used for differential
606   expression analysis with DESeq2 (Love et al., 2014; Liao et al., 2019). Differential gene
607   expression analysis was carried out to account for sex differences: design = ~ Sex + Condition.
608   Differentially expressed genes (DEGs) were defined as |Log$_2$FC>0.5|, adj. p-value<0.05.

609   *Spatial RNA sequencing Pipeline*

610   Spatial RNA sequencing data was analyzed according to previously published 10X protocols.
611   Briefly, FASTQ files were obtained from the 10X Space Ranger's mkfastq pipeline. Space
612   Ranger count pipeline was used align H&E-images and barcode count information and
613   reference transcriptome (GENCODE release 38). Neuron, Surrounding and Other barcodes
614   were identified as previously described (Tavares-Ferreira et al., 2022). Cloupe files were
615   obtained to illustrate gene expression in a spatial context. Differential gene expression analysis
616   was carried out with DESeq2 as described in Single-Nucleus RNA sequencing pipeline. Neuron
617   cell diameter was measured from H&E images in CellSens.

618   *CONOS cell subtype predictions*

619   Label propagation from previously published lumbar data to the C2 data was performed with the
620   R package conos v1.5.2 (Barkas et al., 2019). A conos object was built on the corresponding,
621   processed RNA assays with basicSeuratProc, using umap = TRUE. A graph was then built in
622   CCA space with the following parameters: con$buildGraph(k=30, k.self=5, space='CCA',
623   ncomps=40, n.odgenes=2000, matching.method='mNN', #balance.edge.weights = TRUE,
624   metric='angular', score.component.variance=TRUE, verbose=TRUE). Cell cluster communities
625   and graph embeddings were processed with default settings, prior to label propagation with
626   defaults con$propagateLabels. Labels were then back propagated to the Seurat object
627   metadata for comparisons against initial cluster annotations and downstream processing.

628   *Neural Net Cell Type Predictions*

629  Cell types were predicted using a neural net algorithm through the scCAMEL package, as
630  previously described for hDRG (Hu et al., 2022; Yu et al., 2024). Processed RNA-seq data was
631  extracted from the relevant Seurat objects, including previously published spatial-seq (Tavares-
632  Ferreira et al., 2022) and a cross-species harmonized atlas (Bhuiyan et al., 2024). For the latter,
633  human barcodes were extracted, and gene names were converted from mouse to human with
634  the biomaRt package (R).

635  Count and metadata were reassembled into AnnData objects in python for processing. Large
636  clusters were downsampled to the mean (cluster size) +0.5*std to minimize a size bias. Data
637  were then filtered for low expression and cell cycle genes prior to normalization in line with the
638  scCAMEL documentation. Hyperparameter tuning was performed with Optuna using the C2
639  scRNA-seq data as the test/train datasets (learningRate=0.01537, optimizerMmentum=0.8951,
640  dropout=0.42, https://arxiv.org/abs/1907.10902). After tuning, cell type predictions were
641  performed against lumbar (visium) as well as lumbar, thoracic, and TG (harmonized) datasets.

642  *Interactome Analysis*

643  Previously published curated ligand receptor database (Wangzhou et al., 2021), was intersected
644  with the single-nucleus RNA-seq data to identify mechanisms by which DRG endothelial cells,
645  fibroblasts, and myelinating Schwann cells may signal to neurons. Cells for each non-neuronal
646  cell type and neuronal subpopulation were pseudobulked and the expression (in counts per
647  million) of all genes for each cell type was determined. The database was used to identify ligand
648  genes that are expressed in each non-neuronal cell type, and corresponding receptors
649  expressed in DRG neuron populations. Genes were considered expressed in a cell type if they
650  were above the 20th percentile among all genes, as this threshold conservatively differentiated
651  non- and lowly-expressed genes from highly expressed genes in kernel density plots of gene
652  expression generated for each cell type. Additionally, ligand genes were filtered to include only
653  those which were differently expressed (padj < 0.1) and upregulated in samples from chronic
654  pain donors. The resulting interactome table includes 236 interactions between the non-
655  neuronal cell types and each individual neuron subtype. SankeyMATIC was used to visualize
656  the unique ligand-receptor interactions, and the ComplexHeatmap v.2.20.0 R package was used
657  to visualize the expression of ligand and receptor genes. R v4.4.2 was used for all calculations
658  and interactome generation.

659  *Figure Generation*

660  Figures were compiled in Inkscape, GraphPad Prism 10 (GraphPad Software, Inc. San Diego,
661  CA USA), RStudio v.2024.12.0 and Adobe Illustrator 2024.
662  **Data availability**
663  Processed data will be publicly accessible on the SPARC portal.
664
665

16

## References

Ahlstrom FHG, Viisanen H, Karhinen L, Velagapudi V, Blomqvist KJ, Lilius TO, Rauhala PV, Kalso EA (2024) Gene expression in the dorsal root ganglion and the cerebrospinal fluid metabolome in polyneuropathy and opioid tolerance in rats. IBRO Neurosci Rep 17:38-51.

Amadesi S, Grant AD, Cottrell GS, Vaksman N, Poole DP, Rozengurt E, Bunnett NW (2009) Protein kinase D isoforms are expressed in rat and mouse primary sensory neurons and are activated by agonists of protease-activated receptor 2. J Comp Neurol 516:141-156.

Amemiya HM, Kundaje A, Boyle AP (2019) The ENCODE Blacklist: Identification of Problematic Regions of the Genome. Scientific Reports 9:9354.

Arendt-Nielsen L, Brennum J, Sindrup S, Bak P (1994) Electrophysiological and psychophysical quantification of temporal summation in the human nociceptive system. Eur J Appl Physiol Occup Physiol 68:266-273.

Asaithambi A, Kanthasamy A, Saminathan H, Anantharam V, Kanthasamy AG (2011) Protein kinase D1 (PKD1) activation mediates a compensatory protective response during early stages of oxidative stress-induced neuronal degeneration. Molecular Neurodegeneration 6:43.

Backonja MM et al. (2013) Value of quantitative sensory testing in neurological and pain disorders: NeuPSIG consensus. Pain 154:1807-1819.

Bali KK, Venkataramani V, Satagopam VP, Gupta P, Schneider R, Kuner R (2013) Transcriptional Mechanisms Underlying Sensitization of Peripheral Sensory Neurons by Granulocyte-/Granulocyte-Macrophage Colony Stimulating Factors. Molecular Pain 9:1744-8069-1749-1748.

Barkas N, Petukhov V, Nikolaeva D, Lozinsky Y, Demharter S, Khodosevich K, Kharchenko PV (2019) Joint analysis of heterogeneous single-cell RNA-seq dataset collections. Nature Methods 16:695-698.

Belonogova NM, Elgaeva EE, Zorkoltseva IV, Kirichenko AV, Svishcheva GR, Freidin MB, Williams FMK, Suri P, Axenovich TI, Tsepilov YA (2025) A multi-trait approach identified 7 novel genes for back pain. Pain Rep 10:e1218.

Bhuiyan SA et al. (2024) Harmonized cross-species cell atlases of trigeminal and dorsal root ganglia. Science Advances 10:eadj9173.

Bogduk N, Govind J (2009) Cervicogenic headache: an assessment of the evidence on clinical diagnosis, invasive tests, and treatment. Lancet Neurol 8:959-968.

Calvo M, Zhu N, Grist J, Ma Z, Loeb JA, Bennett DL (2011) Following nerve injury neuregulin-1 drives microglial proliferation and neuropathic pain via the MEK/ERK pathway. Glia 59:554-568.

Cherif H, Mannarino M, Pacis AS, Ragoussis J, Rabau O, Ouellet JA, Haglund L (2022) Single-Cell RNA-Seq Analysis of Cells from Degenerating and Non-Degenerating Intervertebral Discs from the Same Individual Reveals New Biomarkers for Intervertebral Disc Degeneration. International Journal of Molecular Sciences 23:3993.

Conn KJ, Gao W, McKee A, Lan MS, Ullman MD, Eisenhauer PB, Fine RE, Wells JM (2004) Identification of the protein disulfide isomerase family member PDIp in experimental Parkinson's disease and Lewy body pathology. Brain Research 1022:164-172.

Cruccu G, Sommer C, Anand P, Attal N, Baron R, Garcia-Larrea L, Haanpaa M, Jensen TS, Serra J, Treede RD (2010) EFNS guidelines on neuropathic pain assessment: revised 2009. Eur J Neurol 17:1010-1018.

Dai D-W, Xu Z, Chen X, Yuan L, Zhang A-J, Zhang P-Q, Lu Y-M, Deng Z-F (2014) Distinct roles of neuregulin in different models of neuropathic pain. Neurological Sciences 35:531-536.

714 Dang D, Ye Y, Aouizerat BE, Patel YK, Viet DT, Chan KC, Ono K, Doan C, Figueroa JD, Yu G,
715     Viet CT (2020) Targeting the endothelin axis as a therapeutic strategy for oral cancer
716     metastasis and pain. Scientific Reports 10:20832.
717 David ET, Yousuf MS, Mei HR, Jain A, Krishnagiri S, Elahi H, Venkatesan R, Srikanth KD,
718     Dussor G, Dalva MB, Price TJ (2024) ephrin-B2 promotes nociceptive plasticity and
719     hyperalgesic priming through EphB2-MNK-eIF4E signaling in both mice and humans.
720     Pharmacol Res 206:107284.
721 Davies P, Bailey PJ, Goldenberg MM, Ford-Hutchinson AW (1984) The Role of Arachidonic Acid
722     Oxygenation Products in Pain and Inflammation. Annual Review of Immunology 2:335-
723     357.
724 De Rossi P, Harde E, Dupuis JP, Martin L, Chounlamountri N, Bardin M, Watrin C, Benetollo C,
725     Pernet-Gallay K, Luhmann HJ, Honnorat J, Malleret G, Groc L, Acker-Palmer A, Salin
726     PA, Meissirel C (2016) A critical role for VEGF and VEGFR2 in NMDA receptor synaptic
727     function and fear-related behavior. Molecular Psychiatry 21:1768-1780.
728 Dobin A, Gingeras TR (2015) Mapping RNA-seq Reads with STAR. Curr Protoc Bioinformatics
729     51:11 14 11-11 14 19.
730 Dworkin RH et al. (2005) Core outcome measures for chronic pain clinical trials: IMMPACT
731     recommendations. Pain 113:9-19.
732 Elazar N, Vainshtein A, Golan N, Vijayaragavan B, Schaeren-Wiemers N, Eshed-Eisenbach Y,
733     Peles E (2019) Axoglial Adhesion by Cadm4 Regulates CNS Myelination. Neuron
734     101:224-231.e225.
735 Freidin MB, Tsepilov YA, Palmer M, Karssen LC, Suri P, Aulchenko YS, Williams FMK (2019)
736     Insight into the genetic architecture of back pain and its risk factors from a study of
737     509,000 individuals. Pain 160:1361-1373.
738 Fundaun J, Ridehalgh C, Koushesh S, Novak A, Tejos-Bravo M, Bremner S, Baskozos G, Dilley
739     A, Schmid AB (2025) The presence and prognosis of nerve pathology following whiplash
740     injury: a prospective cohort study. Brain.
741 Geranton SM (2019) Does epigenetic 'memory' of early-life stress predispose to chronic pain in
742     later life? A potential role for the stress regulator FKBP5. Philos Trans R Soc Lond B Biol
743     Sci 374:20190283.
744 Goadsby PJ, Edvinsson L, Ekman R (1990) Vasoactive peptide release in the extracerebral
745     circulation of humans during migraine headache. Annals of Neurology 28:183-187.
746 Guan Z, Kuhn JA, Wang X, Colquitt B, Solorzano C, Vaman S, Guan AK, Evans-Reinsch Z,
747     Braz J, Devor M, Abboud-Werner SL, Lanier LL, Lomvardas S, Basbaum AI (2016)
748     Injured sensory neuron-derived CSF1 induces microglial proliferation and DAP12-
749     dependent pain. Nat Neurosci 19:94-101.
750 Hofstetter CT, Nguyen; Payne, Cathryn (2025) Human Tissue Procurement from Atlanto-Axial
751     Fusion Surgery. protocolsio.
752 Hu Y, Jiang Y, Behnan J, Ribeiro MM, Kalantzi C, Zhang MD, Lou D, Häring M, Sharma N,
753     Okawa S, Del Sol A, Adameyko I, Svensson M, Persson O, Ernfors P (2022) Neural
754     network learning defines glioblastoma features to be of neural crest perivascular or
755     radial glia lineages. Sci Adv 8:eabm6340.
756 Hummig W, Baggio DF, Lopes RV, Dos Santos SMD, Ferreira LEN, Chichorro JG (2023)
757     Antinociceptive effect of ultra-low dose naltrexone in a pre-clinical model of
758     postoperative orofacial pain. Brain Res 1798:148154.
759 Islam B, Stephenson J, Young B, Manca M, Buckley DA, Radford H, Zis P, Johnson MI, Finn DP,
760     McHugh PC (2022) The Identification of Blood Biomarkers of Chronic Neuropathic Pain
761     by Comparative Transcriptomics. Neuromolecular Med 24:320-338.
762 Iwasa T, Afroz S, Inoue M, Arakaki R, Oshima M, Raju R, Waskitho A, Inoue M, Baba O,
763     Matsuka Y (2019) IL-10 and CXCL2 in trigeminal ganglia in neuropathic pain. Neurosci
764     Lett 703:132-138.

765   Ji R-R, Chamessian A, Zhang Y-Q (2016) Pain regulation by non-neuronal cells and
766         inflammation. Science 354:572-577.
767   Jorgensen JR, Xu XJ, Arnold HM, Munro G, Hao JX, Pepinsky B, Huang C, Gong BJ,
768         Wiesenfeld-Hallin Z, Wahlberg LU, Johansen TE (2012) Meteorin reverses
769         hypersensitivity in rat models of neuropathic pain. Exp Neurol 237:260-266.
770   Jørgensen JR, Xu X-J, Arnold HM, Munro G, Hao J-X, Pepinsky B, Huang C, Gong BJ,
771         Wiesenfeld-Hallin Z, Wahlberg LU, Johansen TE (2012) Meteorin reverses
772         hypersensitivity in rat models of neuropathic pain. Experimental Neurology 237:260-266.
773   Jung M, Dourado M, Maksymetz J, Jacobson A, Laufer BI, Baca M, Foreman O, Hackos DH,
774         Riol-Blanco L, Kaminker JS (2023) Cross-species transcriptomic atlas of dorsal root
775         ganglia reveals species-specific programs for sensory function. Nat Commun 14:366.
776   Keller JT, Saunders MC, Beduk A, Jollis JG (1985) Innervation of the posterior fossa dura of the
777         cat. Brain Res Bull 14:97-102.
778   Kobayashi K, Fukuoka T, Obata K, Yamanaka H, Dai Y, Tokunaga A, Noguchi K (2005) Distinct
779         expression of TRPM8, TRPA1, and TRPV1 mRNAs in rat primary afferent neurons with
780         adelta/c-fibers and colocalization with trk receptors. J Comp Neurol 493:596-606.
781   Lacagnina MJ et al. (2024) B cells drive neuropathic pain–related behaviors in mice through
782         IgG–Fc gamma receptor signaling. Science Translational Medicine 16:eadj1277.
783   Lafta MS, Sokolov AV, Landtblom AM, Ericson H, Schioth HB, Abu Hamdeh S (2024) Exploring
784         biomarkers in trigeminal neuralgia patients operated with microvascular decompression:
785         A comparison with multiple sclerosis patients and non-neurological controls. Eur J Pain
786         28:929-942.
787   Lee MC, McCubbin JA, Christensen AD, Poole DP, Rajasekhar P, Lieu T, Bunnett NW, Garcia-
788         Caraballo S, Erickson A, Brierley SM, Saleh R, Achuthan A, Fleetwood AJ, Anderson RL,
789         Hamilton JA, Cook AD (2017) G-CSF Receptor Blockade Ameliorates Arthritic Pain and
790         Disease. J Immunol 198:3565-3575.
791   Li S, Brimmers A, van Boekel RLM, Vissers KCP, Coenen MJH (2023) A systematic review of
792         genome-wide association studies for pain, nociception, neuropathy, and pain treatment
793         responses. Pain 164:1891-1911.
794   Li Y, Uhelski ML, North RY, Mwirigi JM, Tatsui CE, McDonough KE, Cata JP, Corrales G, Dussor
795         G, Price TJ, Dougherty PM (2024) Tomivosertib reduces ectopic activity in dorsal root
796         ganglion neurons from patients with radiculopathy. Brain 147:2991-2997.
797   Liao Y, Smyth GK, Shi W (2019) The R package Rsubread is easier, faster, cheaper and better
798         for alignment and quantification of RNA sequencing reads. Nucleic Acids Research
799         47:e47-e47.
800   Lin W et al. (2019) Function of CSF1 and IL34 in Macrophage Homeostasis, Inflammation, and
801         Cancer. Front Immunol 10:2019.
802   Linnstaedt SD, Riker KD, Rueckeis CA, Kutchko KM, Lackey L, McCarthy KR, Tsai YH, Parker
803         JS, Kurz MC, Hendry PL, Lewandowski C, Datner E, Pearson C, O'Neil B, Domeier R,
804         Kaushik S, Laederach A, McLean SA (2018) A Functional riboSNitch in the 3'
805         Untranslated Region of FKBP5 Alters MicroRNA-320a Binding Efficiency and Mediates
806         Vulnerability to Chronic Post-Traumatic Pain. J Neurosci 38:8407-8420.
807   Lisi V, Garbo G, Battistella P, Micciche F, Stecca A, Terrazzino S, Franzoi M, Tripoli E, Leon A,
808         Clementi M (2006) Endothelin receptor A -231 G>A polymorphism: no linkage to primary
809         pediatric headache. Headache 46:486-491.
810   Love MI, Huber W, Anders S (2014) Moderated estimation of fold change and dispersion for
811         RNA-seq data with DESeq2. Genome Biology 15:550.
812   Lu J, Ebraheim NA (1998) Anatomic considerations of C2 nerve root ganglion. Spine (Phila Pa
813         1976) 23:649-652.
814   Lu Q, Xu Y, Zhang Z, Li S, Zhang Z (2023) Primary hypertrophic osteoarthropathy: genetics,
815         clinical features and management. Front Endocrinol (Lausanne) 14:1235040.

Maiaru M, Acton RJ, Wozniak EL, Mein CA, Bell CG, Geranton SM (2023) A DNA methylation signature in the stress driver gene Fkbp5 indicates a neuropathic component in chronic pain. Clin Epigenetics 15:155.

Maiarù M, Morgan OB, Mao T, Breitsamer M, Bamber H, Pöhlmann M, Schmidt MV, Winter G, Hausch F, Géranton SM (2018) The stress regulator FKBP51: a novel and promising druggable target for the treatment of persistent pain states across sexes. Pain 159:1224-1234.

Megat S, Ray PR, Tavares-Ferreira D, Moy JK, Sankaranarayanan I, Wangzhou A, Fang Lou T, Barragan-Iglesias P, Campbell ZT, Dussor G, Price TJ (2019a) Differences between Dorsal Root and Trigeminal Ganglion Nociceptors in Mice Revealed by Translational Profiling. The Journal of Neuroscience 39:6829-6847.

Megat S, Ray PR, Moy JK, Lou TF, Barragan-Iglesias P, Li Y, Pradhan G, Wanghzou A, Ahmad A, Burton MD, North RY, Dougherty PM, Khoutorsky A, Sonenberg N, Webster KR, Dussor G, Campbell ZT, Price TJ (2019b) Nociceptor Translational Profiling Reveals the Ragulator-Rag GTPase Complex as a Critical Generator of Neuropathic Pain. J Neurosci 39:393-411.

Miao J, Wang F, Fang Y (2012) Association of 231G>A polymorphism of endothelin type A receptor gene with migraine: a meta-analysis. J Neurol Sci 323:232-235.

Mitchell ME, Torrijos G, Cook LF, Mwirigi JM, He L, Shiers S, Price TJ (2024) Interleukin-6 induces nascent protein synthesis in human dorsal root ganglion nociceptors primarily via MNK-eIF4E signaling. Neurobiol Pain 16:100159.

Moy JK, Kuhn JL, Szabo-Pardi TA, Pradhan G, Price TJ (2018) eIF4E phosphorylation regulates ongoing pain, independently of inflammation, and hyperalgesic priming in the mouse CFA model. Neurobiol Pain 4:45-50.

Moy JK, Khoutorsky A, Asiedu MN, Black BJ, Kuhn JL, Barragán-Iglesias P, Megat S, Burton MD, Burgos-Vega CC, Melemedjian OK, Boitano S, Vagner J, Gkogkas CG, Pancrazio JJ, Mogil JS, Dussor G, Sonenberg N, Price TJ (2017) The MNK–eIF4E Signaling Axis Contributes to Injury-Induced Nociceptive Plasticity and the Development of Chronic Pain. The Journal of Neuroscience 37:7481-7499.

Nakanishi T, Nakamura Y, Umeno J (2021) Recent advances in studies of SLCO2A1 as a key regulator of the delivery of prostaglandins to their sites of action. Pharmacology & Therapeutics 223:107803.

Nguyen MQ, von Buchholtz LJ, Reker AN, Ryba NJ, Davidson S (2021) Single-nucleus transcriptomic analysis of human dorsal root ganglion neurons. Elife 10.

North R, Yan L, Ray P, Rhines L, Tatsui C, Rao G, Johansson C, Kim YH, Zhang B, Dussor G, Kim TH, Price TJ, Dougherty PM (2019) Electrophysiologic and transcriptomic correlates of neuropathic pain in human dorsal root ganglion neurons. Brain:in press.

Noseda R, Melo-Carrillo A, Nir RR, Strassman AM, Burstein R (2019) Non-Trigeminal Nociceptive Innervation of the Posterior Dura: Implications to Occipital Headache. J Neurosci 39:1867-1880.

Ohlsson L, Kronvall E, Stratton J, Edvinsson L (2018) Fremanezumab blocks CGRP induced dilatation in human cerebral, middle meningeal and abdominal arteries. J Headache Pain 19:66.

Pertea M, Kim D, Pertea GM, Leek JT, Salzberg SL (2016) Transcript-level expression analysis of RNA-seq experiments with HISAT, StringTie and Ballgown. Nature Protocols 11:1650-1667.

Price DD (1972) Characteristics of second pain and flexion reflexes indicative of prolonged central summation. Exp Neurol 37:371-387.

Quinlan AR (2014) BEDTools: The Swiss-Army Tool for Genome Feature Analysis. Current Protocols in Bioinformatics 47:11.12.11-11.12.34.

Rajasekaran S, Soundararajan DCR, Nayagam SM, Tangavel C, Raveendran M, Thippeswamy PB, Djuric N, Anand SV, Shetty AP, Kanna RM (2022) Modic changes are associated with activation of intense inflammatory and host defense response pathways &#x2013; molecular insights from proteomic analysis of human intervertebral discs. The Spine Journal 22:19-38.

Ray PR, Shiers S, Caruso JP, Tavares-Ferreira D, Sankaranarayanan I, Uhelski ML, Li Y, North RY, Tatsui C, Dussor G, Burton MD, Dougherty PM, Price TJ (2023) RNA profiling of human dorsal root ganglia reveals sex differences in mechanisms promoting neuropathic pain. Brain 146:749-766.

Renthal W, Tochitsky I, Yang L, Cheng YC, Li E, Kawaguchi R, Geschwind DH, Woolf CJ (2020) Transcriptional Reprogramming of Distinct Peripheral Sensory Neuron Subtypes after Axonal Injury. Neuron 108:128-144 e129.

Renthal W et al. (2021) Human cells and networks of pain: Transforming pain target identification and therapeutic development. Neuron 109:1426-1429.

Ridehalgh C, Fundaun J, Bremner S, Cercignani M, Koushesh S, Young R, Novak A, Greening J, Schmid AB, Dilley A (2025) Evidence for peripheral neuroinflammation after acute whiplash. Pain.

Safiri S, Kolahi AA, Hoy D, Buchbinder R, Mansournia MA, Bettampadi D, Ashrafi-Asgarabad A, Almasi-Hashiani A, Smith E, Sepidarkish M, Cross M, Qorbani M, Moradi-Lakeh M, Woolf AD, March L, Collins G, Ferreira ML (2020) Global, regional, and national burden of neck pain in the general population, 1990-2017: systematic analysis of the Global Burden of Disease Study 2017. Bmj 368:m791.

Sankaranarayanan I, Tavares-Ferreira D, Mwirigi JM, Mejia GL, Burton MD, Price TJ (2023a) Inducible co-stimulatory molecule (ICOS) alleviates paclitaxel-induced neuropathic pain via an IL-10-mediated mechanism in female mice. J Neuroinflammation 20:32.

Sankaranarayanan I, Tavares-Ferreira D, He L, Kume M, Mwirigi JM, Madsen TM, Petersen KA, Munro G, Price TJ (2023b) Meteorin Alleviates Paclitaxel-Induced Peripheral Neuropathic Pain in Mice. J Pain 24:555-567.

Sankaranarayanan I, Kume M, Mohammed A, Mwirigi JM, Inturi NN, Munro G, Petersen KA, Tavares-Ferreira D, Price TJ (2025) Persistent changes in the dorsal root ganglion nociceptor translatome governs hyperalgesic priming in mice: roles of GPR88 and Meteorin. PAIN:10.1097/j.pain.0000000000003523.

Schweizerhof M, Stösser S, Kurejova M, Njoo C, Gangadharan V, Agarwal N, Schmelz M, Bali KK, Michalski CW, Brugger S, Dickenson A, Simone DA, Kuner R (2009) Hematopoietic colony–stimulating factors mediate tumor-nerve interactions and bone cancer pain. Nature Medicine 15:802-807.

Sharma N, Flaherty K, Lezgiyeva K, Wagner DE, Klein AM, Ginty DD (2020) The emergence of transcriptional identity in somatosensory neurons. Nature 577:392-398.

Shiers S, Klein RM, Price TJ (2020) Quantitative differences in neuronal subpopulations between mouse and human dorsal root ganglia demonstrated with RNAscope in situ hybridization. Pain 161:2410-2424.

Shiers S, Sahn JJ, Price TJ (2023) MNK1 and MNK2 Expression in the Human Dorsal Root and Trigeminal Ganglion. Neuroscience 515:96-107.

Shiers S, Yousuf MS, Mwirigi JM, Cervantes A, Price TJ (2024) Human Ganglia and Spinal Cord Tissue Procurement from Organ Donors and Tissue Quality Assessment. Protocolsio.

Shiers SI, Sankaranarayanan I, Jeevakumar V, Cervantes A, Reese JC, Price TJ (2021) Convergence of peptidergic and non-peptidergic protein markers in the human dorsal root ganglion and spinal dorsal horn. J Comp Neurol 529:2771-2788.

Simmons LJ, Surles-Zeigler MC, Li Y, Ford GD, Newman GD, Ford BD (2016) Regulation of inflammatory responses by neuregulin-1 in brain ischemia and microglial cells in vitro involves the NF-kappa B pathway. Journal of Neuroinflammation 13:237.

917    Solis-Castro OO, Wong N, Boissonade FM (2021) Chemokines and Pain in the Trigeminal
918            System. Front Pain Res (Lausanne) 2:689314.
919    Staud R, Craggs JG, Robinson ME, Perlstein WM, Price DD (2007) Brain activity related to
920            temporal summation of C-fiber evoked pain. Pain 129:130-142.
921    Tarasov A, Vilella AJ, Cuppen E, Nijman IJ, Prins P (2015) Sambamba: fast processing of NGS
922            alignment formats. Bioinformatics 31:2032-2034.
923    Tavares-Ferreira D, Shiers S, Ray PR, Wangzhou A, Jeevakumar V, Sankaranarayanan I,
924            Cervantes AM, Reese JC, Chamessian A, Copits BA, Dougherty PM, Gereau RW,
925            Burton MD, Dussor G, Price TJ (2022) Spatial transcriptomics of dorsal root ganglia
926            identifies molecular signatures of human nociceptors. Science Translational Medicine
927            14:eabj8186.
928    Tokuhiro T, Matsumae G, Endo T, Ogawa Y, Ogawa T, Liyile C, Nishida Y, Alhasan H, Kobayashi
929            H, Ebata T, Shimizu T, Takahashi D, Onodera T, Kadoya K, Terkawi MA, Iwasaki N
930            (2024) Cellular communication network factor 3 contributes to the pathological process
931            of rheumatoid arthritis through promoting cell senescence and osteoclastogenesis in the
932            joint. Journal of Autoimmunity 149:103334.
933    Treede RD et al. (2019) Chronic pain as a symptom or a disease: the IASP Classification of
934            Chronic Pain for the International Classification of Diseases (ICD-11). Pain 160:19-27.
935    Ushach I, Zlotnik A (2016) Biological role of granulocyte macrophage colony-stimulating factor
936            (GM-CSF) and macrophage colony-stimulating factor (M-CSF) on cells of the myeloid
937            lineage. J Leukoc Biol 100:481-489.
938    Usoskin D, Furlan A, Islam S, Abdo H, Lonnerberg P, Lou D, Hjerling-Leffler J, Haeggstrom J,
939            Kharchenko O, Kharchenko PV, Linnarsson S, Ernfors P (2015) Unbiased classification
940            of sensory neuron types by large-scale single-cell RNA sequencing. Nat Neurosci
941            18:145-153.
942    Walton DM, MacDermid JC (2013) A brief 5-item version of the Neck Disability Index shows
943            good psychometric properties. Health Qual Life Outcomes 11:108.
944    Wangzhou A, Paige C, Neerukonda SV, Naik DK, Kume M, David ET, Dussor G, Ray PR, Price
945            TJ (2021) A ligand-receptor interactome platform for discovery of pain mechanisms and
946            therapeutic targets. Sci Signal 14.
947    Wu A-M et al. (2024) Global, regional, and national burden of neck pain, 1990–2020,
948            and projections to 2050: a systematic analysis of the Global Burden of Disease Study
949            2021. The Lancet Rheumatology 6:e142-e155.
950    Xie JY, Qu C, Munro G, Petersen KA, Porreca F (2019) Antihyperalgesic effects of Meteorin in
951            the rat chronic constriction injury model: a replication study. Pain 160:1847-1855.
952    Yang L, Xu M, Bhuiyan SA, Li J, Zhao J, Cohrs RJ, Susterich JT, Signorelli S, Green U, Stone
953            JR, Levy D, Lennerz JK, Renthal W (2022) Human and mouse trigeminal ganglia cell
954            atlas implicates multiple cell types in migraine. Neuron 110:1806-1821 e1808.
955    Yu H et al. (2024) Leveraging deep single-soma RNA sequencing to explore the neural basis of
956            human somatosensation. Nature Neuroscience 27:2326-2340.
957    Zeisel A, Hochgerner H, Lonnerberg P, Johnsson A, Memic F, van der Zwan J, Haring M, Braun
958            E, Borm LE, La Manno G, Codeluppi S, Furlan A, Lee K, Skene N, Harris KD, Hjerling-
959            Leffler J, Arenas E, Ernfors P, Marklund U, Linnarsson S (2018) Molecular Architecture of
960            the Mouse Nervous System. Cell 174:999-1014 e1022.
961    Zeng J, Lai C, Luo J, Li L (2023) Functional investigation and two-sample Mendelian
962            randomization study of neuropathic pain hub genes obtained by WGCNA analysis. Front
963            Neurosci 17:1134330.
964    Zhou QL, Strichartz G, Davar G (2001) Endothelin-1 activates ET(A) receptors to increase
965            intracellular calcium in model sensory neurons. Neuroreport 12:3853-3857.

966    Zhou Z, Davar G, Strichartz G (2002) Endothelin-1 (ET-1) selectively enhances the activation
967            gating of slowly inactivating tetrodotoxin-resistant sodium currents in rat sensory
968            neurons: a mechanism for the pain-inducing actions of ET-1. J Neurosci 22:6325-6330.
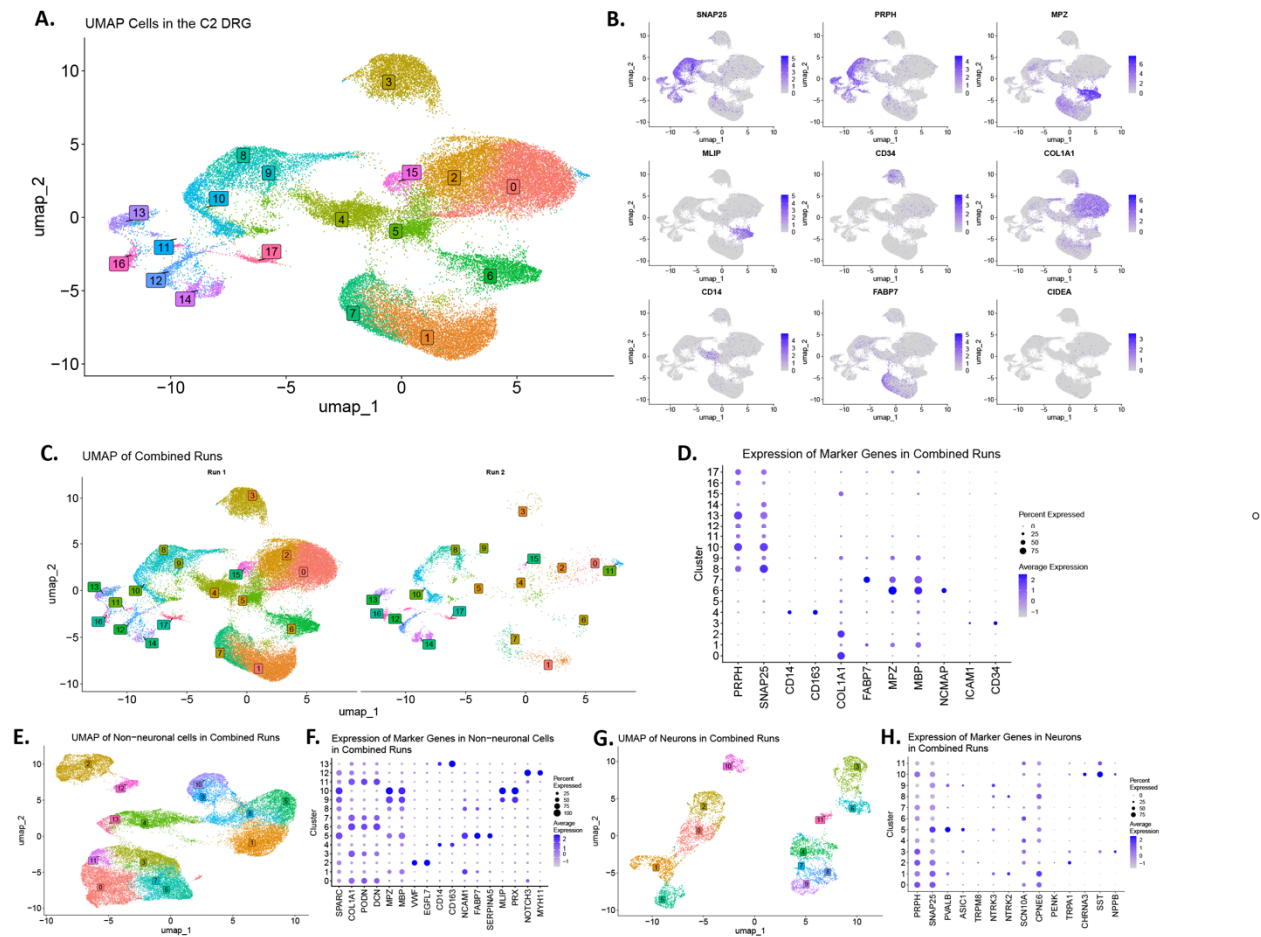
969

970

**Figure Legends:**



972

**Figure 1: Cell types identified in C2 DRGs using single-nuc RNAseq. A.** UMAP plot with 18 clusters identified in 12 DRGs from 12 patients. **B.** UMAP plots showing expression of marker genes used to identify neuronal (*SNAP25, PRPH*) and non-neuronal (*MPZ, MLIP, CD34, COL1A1, CD14, FABP7, CIDEA*) cell populations. **C.** Split UMAP showing cell populations identified in 2 runs of single-nuc RNAseq. **D.** Dot plot showing expression of marker genes across the 18 clusters of cells. **E.** UMAP of 14 non-neuronal cell clusters identified by expression of non-neuronal marker genes. **F.** Dot plot of expression of non-neuronal marker genes across 14 non-neuronal clusters. **G.** UMAP of 12 clusters of neuronal cells identified by enrichment of neuronal marker gene expression. **H.** Dot plot of expression of neuronal marker genes across 12 neuronal clusters.
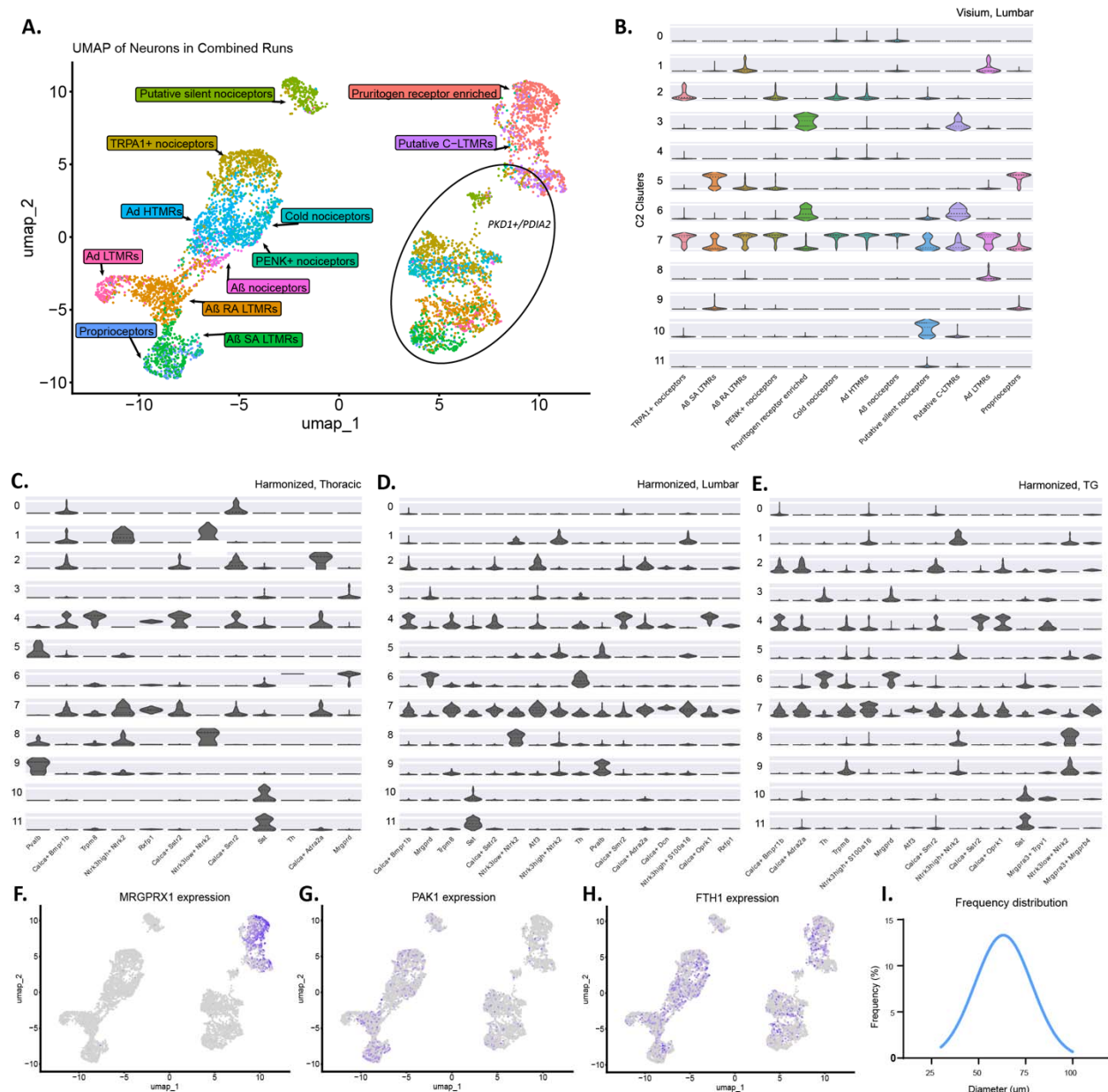
**Figure 2: Characterization of neuronal cell subtypes identified in C2 DRG compared to lumbar, thoracic and trigeminal ganglia. A.** UMAP of neuronal clusters with labels from lumbar DRGs identified with spatial transcriptomics. Cells with enrichment of *PKD1* and *PDIA2* are circled. **B.** Violin plot showing the proportional expression of lumbar DRG subtypes identified with spatial transcriptomics in Tavares-Ferreira & Shiers' atlas, in each neuronal cluster in the C2 DRG. **C-E.** Violin plot showing the proportional expression of thoracic DRG (**C.**), lumbar DRG (**D.**), or trigeminal ganglia (**E.**) subtypes labeled with single-nuc RNAseq in Bhuiyan et al.'s atlas, in each neuronal cluster in the C2 DRG. **F-H.** UMAP plots showing expression of genes *MRGPRX1* (**F.**), *PAK1* (**G.**) and *FTH1* (**H.**). **I.** Diameters of neurons was measured from H&E-stained images of C2 DRGs and the frequency of diameters was shown (in micrometers). Gaussian curve fits are shown for visualization purposes.

25

995
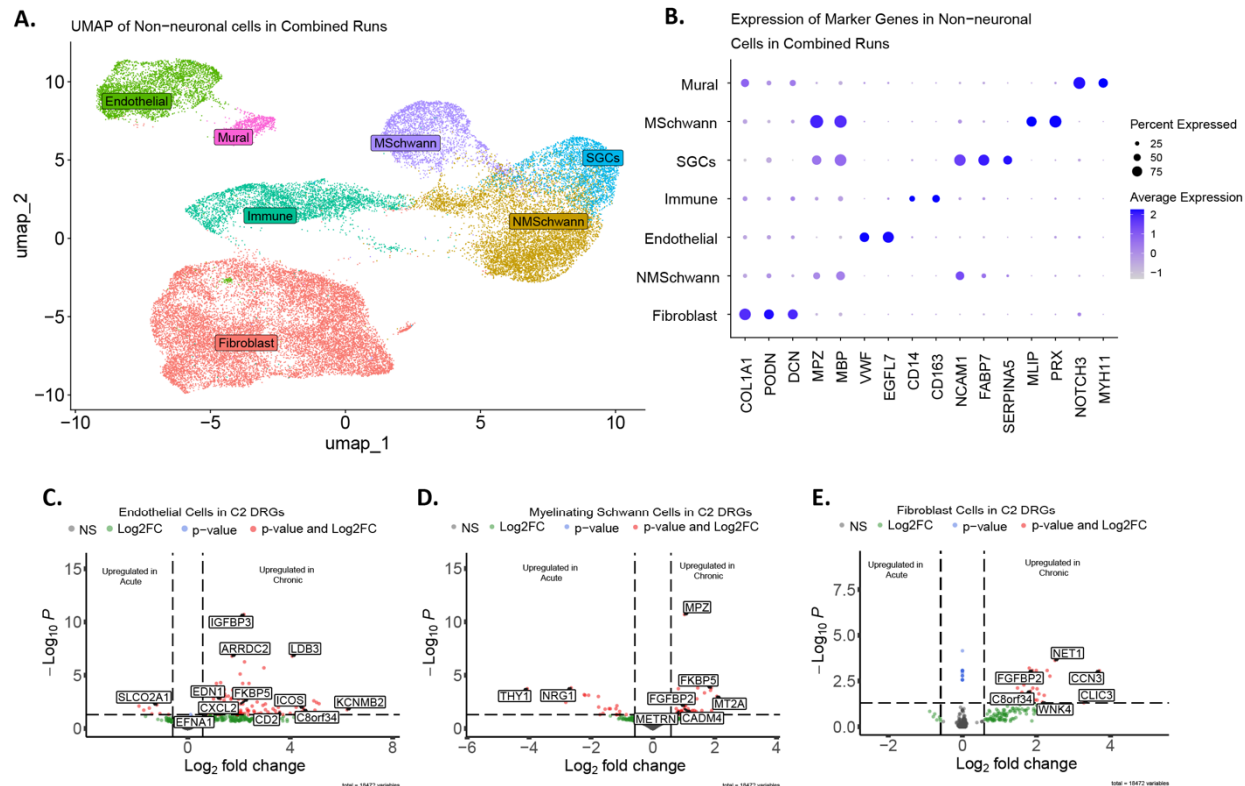
**Figure 3: Characterization of non-neuronal cell subtypes identified in C2 DRGs and molecular differences attributed to pain phenotype. A.** UMAP of non-neuronal clusters labeled through enriched expression of marker genes. **B.** Dot plot showing expression of markers defining non-neuronal cell clusters. **C-E.** Volcano plot showing differential gene expression patterns when comparing samples from acute and chronic patients in endothelial cells (**C.**), myelinating Schwann cells (**D.**) and fibroblast cells (**E.**). Differentially expressed genes (DEGs) were defined as genes with adj. p-value<0.05 and |Log$_2$FC|>0.5 and illustrated by red dots.

26

**A.** Differentially expressed genes identified with bulk RNAseq in C2 DRGs

**B.** Differentially expressed genes in bulk and single-nucleus sequencing



|  | Bulk RNAseq | | Endothelial Cells single-nuc RNAseq | | Myelinating Schwann Cells single-nuc RNAseq | | Fibroblast Cells single-nuc RNAseq | |
|---|---|---|---|---|---|---|---|---|
| Gene | Log2FC | adj p-value | Log2FC | adj p-value | Log2FC | adj p-value | Log2FC | adj p-value |
| C8orf34 | 0.019 | 0.504 | 4.533 | 0.017 | N/A | N/A | 1.836 | 0.011 |
| GADD45B | -0.014 | 0.518 | 1.753 | 0.000 | N/A | N/A | 1.901 | 0.008 |
| FGFBP2 | -0.020 | 0.442 | 0.056 | 0.685 | 1.020 | 0.008 | 1.886 | 0.001 |
| SLCO2A1 | -0.837 | 0.015 | -1.208 | 0.006 | N/A | N/A | 0.020 | 1.000 |
| KLF15 | 0.014 | 0.605 | 2.557 | 0.000 | 1.155 | 0.022 | 0.001 | 1.000 |
| FKBP5 | 0.003 | 0.897 | 2.058 | 0.005 | 1.887 | 0.000 | 0.000 | 1.000 |
| HSPA2 | -0.015 | 0.805 | 1.256 | 0.048 | 1.424 | 0.002 | 0.050 | 1.000 |
| SEC14L1 | 0.018 | 0.718 | 1.085 | 0.005 | 1.089 | 0.025 | -0.008 | 1.000 |

RNA expression in C2 DRGs measured with Visium spatial transcriptomics

Normalized expression in sample 27 (acute)

Normalized expression in sample 26 (chronic)

**C.** SNAP25

**D.** SNAP25 expression

**E.** METRN

**F.** METRN expression

**G.** FGFBP2

**H.** FGFBP2 expression

**I.** SLCO2A1

**J.** SLCO2A1 expression

1004

27

**Figure 4: Identifying transcriptome differences in acute and chronic pain samples with bulk and spatial RNAsequencing. A.** Volcano plot showing differential gene expression patterns identified with bulk RNAsequencing (RNAseq) of 17 DRGs from 13 patients. 40 differentially expressed genes (DEGs) were defined as genes with adj. p-value<0.05 and |Log$_2$FC|>0.5 and illustrated by red dots. 17 genes were upregulated in chronic pain and 23 in acute pain including *SLCO2A1*. **B.** Venn diagram showing the overlap of DEGs identified with bulk RNAseq and snRNAseq. Eight DEGs were identified with more than 1 sequencing approach. **C.** Violinplot of expression of SNAP25 identified with Visium spatial RNAseq. SNAP25 is most highly expressed in Neuron barcodes with minor expression in Surrounding barcodes. **D.** Expression of *SNAP25* barcodes shown in red in a sample from a patient with acute pain (27) and a patient with chronic pain (26). **E.** Violinplot of expression of *METRN* identified with Visium spatial RNAseq. *METRN* is most highly expressed in Neuron barcodes. **F.** Expression of *METRN* barcodes shown in red in a sample from a patient with acute pain (27) and a patient with chronic pain (26) near *SNAP25+* barcodes. **G.** Violinplot of expression of *FGFBP2* identified with Visium spatial RNAseq. *FGFBP2* is most highly expressed in Other barcodes. **H.** Expression of *FGFBP2* barcodes shown in red in a sample from a patient with acute pain (27) and a patient with chronic pain (26) near *SNAP25+* barcodes. **I.** Violinplot of expression of *SLCO2A1* identified with Visium spatial RNAseq. *SLCO2A1* is most highly expressed in Other barcodes. **J.** Expression of *SLCO2A1* barcodes shown in red in a sample from a patient with acute pain (27) and a patient with chronic pain (26).

28

1025



1026
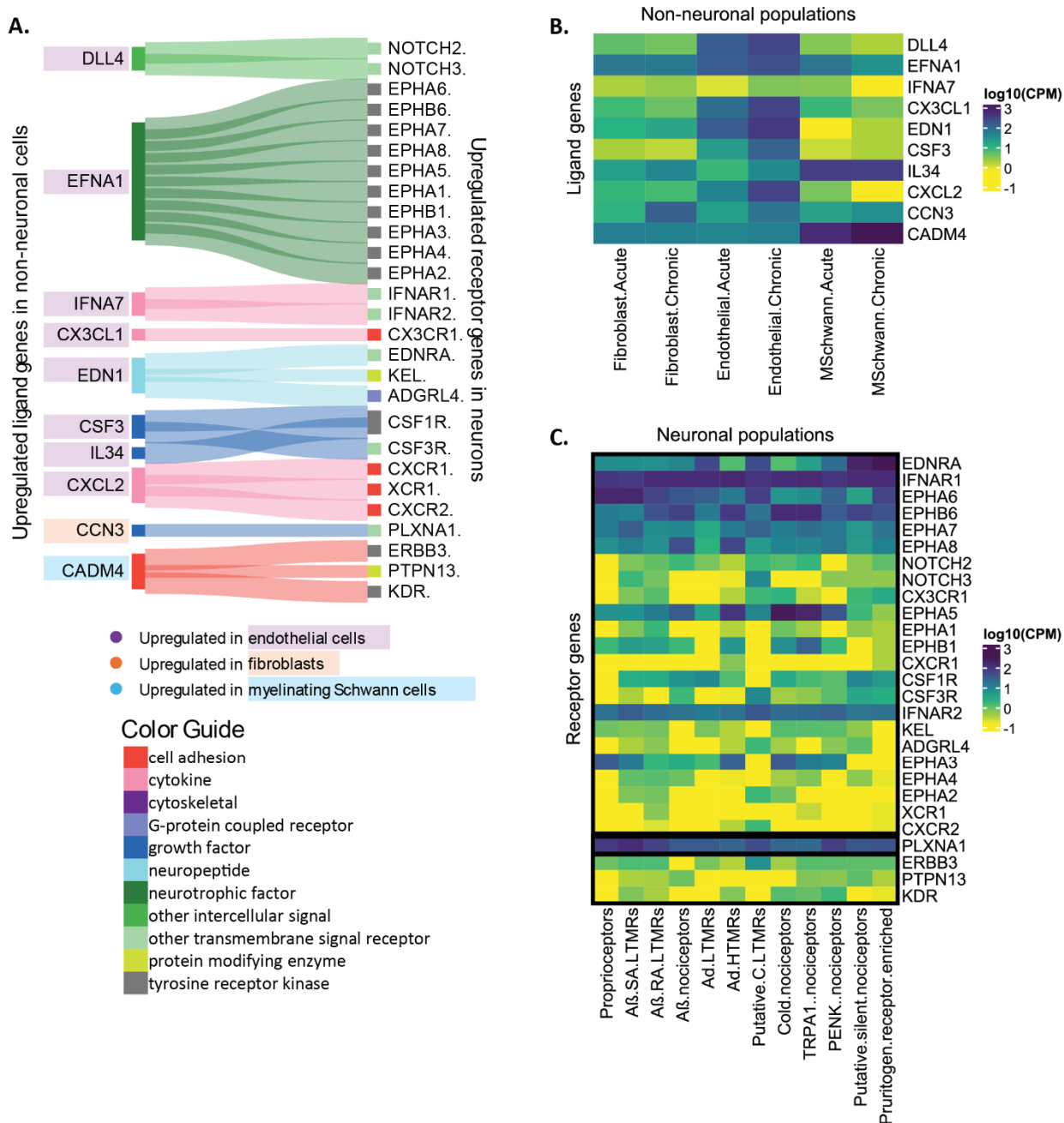
**Figure 5: Interactome analysis showing interactions between ligands released from non-neuronal cells in chronic pain states and receptors in neurons. A.** Sankey diagram showing predicted interactions between ligands released from non-neuronal cells in chronic pain states (defined as genes with adj. p-value<0.1 and |Log$_2$FC|>0.5) and receptors expressed in neurons. **B.** Heatmap showing the expression of ligands expressed in non-neuronal cells in acute and chronic pain samples. **C.** Heatmap showing the expression of receptors expressed in neuronal cells.

1034

1035   **Tables:**

## Table 1: Demographic and clinical characteristics

| | All (N= 22) | Acute pain (N= 11) | Chronic pain (N=11) |
|---|---|---|---|
| **Age** | | | |
| Mean (SD) | 71.73 (12.44) | 77.73 (10.74) | 65.73 (11.41) |
| Median (IQR) | 70.50 (63.00-84.00) | 83.00 (64.00-88.00) | 63.00 (57.00-79.00) |
| **Gender, n (%)** | | | |
| Female | 9 (40.91) | 5 (45.45) | 4 (36.36) |
| Male | 13 (59.09) | 6 (54.55) | 7 (63.64) |
| **Body-mass Index (BMI)** | | | |
| Mean (SD) | 28.76 (10.00) | 26.27 (3.57) | 31.25 (13.55) |
| Median (IQR) | 26.54 (23.44-30.53) | 24.41 (23.20-30.22) | 27.18 (23.94-33.73) |
| **Race, n (%)** | | | |
| White | 18 (81.82) | 10 (90.91) | 8 (72.73) |
| Native American/Alaska Native | 1 (4.55) | 0 (0.00) | 1 (9.09) |
| Asian/ Pacific Islander | 2 (9.09) | 1 (9.09) | 1 (9.09) |
| Unknown | 1 (4.55) | 0 (0.00) | 1 (9.09) |
| **Ethnicity, n (%)** | | | |
| Hispanic or Latino | 0 (0.0) | 0 (0.0) | 0 (0.0) |
| Non-Hispanic or Latino | 21 (95.45) | 11 (100.00) | 10 (90.91) |
| Unknown | 1 (4.55) | 0 (0.0) | 1 (9.09) |
| **Use of opioids in past 6 months, n (%)** | | | |
| No | 15 (68.18) | 8 (72.73) | 7 (63.64) |
| Yes | 4 (18.18) | 1 (9.09) | 3 (27.27) |
| Missing | 3 (13.64) | 2 (18.18) | 1 (9.09) |
| **Location of Pain, n (%)** | | | |
| Bilateral pain | 15 (68.18) | 8 (72.73) | 7 (63.64) |
| Unilateral pain | 4 (18.18) | 2 (18.18) | 2 (18.18) |
| Predominantly unilateral pain* | 1 (4.55) | 0 (0.0) | 1 (9.09) |
| Missing | 2 (9.09) | 1 (9.09) | 1 (9.09) |
| **Duration of neck pain, days** | | | |
| Mean (SD) | 193.25 (300.67) | 5.82 (13.37) | 380.68 (335.22) |
| Median (IQR) | 1.00 (1.00-3.00) | 1.00 (1.00-3.00) | 261.00 (169.00-547.50) |
| **Pain in last 24 hours on most painful side**** | | | |
| Mean (SD) | 5.38 (3.27) | 5.75 (3.68) | 5.05 (3.00) |
| Median (IQR) | 6.00 (3.50-8.00) | 6.50 (2.00-9.00) | 4.50 (3.50-8.00) |
| Missing, n (%) | 1 (4.55) | 1 (9.09) | 0 (0.0) |
| **Neck Disability Index (short form)** | | | |

| | | | |
|---|---|---|---|
| Mean (SD) | 13.95 (6.36) | 16.78 (6.36) | 11.40 (5.46) |
| Median (IQR) | 13.00 (9.00-21.00) | 20.00 (13.00-21.00) | 12.00 (8.00-14.00) |
| Missing, n (%) | 3 (13.64) | 2 (18.18) | 1 (9.09) |

1036

## Table 2: Somatosensory measures

| | All (N= 22) | Acute (N= 11) | Chronic (N=11) |
|---|---|---|---|
| **Brush intensity (0-10)** | | | |
| Mean (SD) | 4.88 (3.34) | 5.50 (3.78) | 4.33 (3.01) |
| Median (IQR) | 4.00 (2.00-9.00) | 5.00 (2.00-9.50) | 4.00 (2.00-5.00) |
| Missing, n (%) | 5 (22.73) | 3 (27.27) | 2 (18.18) |
| **Brush pain, n (%)** | | | |
| No | 16 (72.73) | 7 (63.64) | 9 (81.82) |
| Yes | 1 (4.55) | 1 (9.09) | 0 (0.0) |
| Missing | 5 (22.73) | 3 (27.27) | 2 (18.18) |
| **Light pressure intensity (0-10)** | | | |
| Mean (SD) | 3.21 (2.85) | 3.31 (3.26) | 3.11 (2.62) |
| Median (IQR) | 2.00 (1.00-5.00) | 2.25 (1.00-5.00) | 2.00 (1.00-4.00) |
| Missing, n (%) | 5 (22.73) | 3 (27.27) | 2 (18.18) |
| **Light pressure pain, n (%)** | | | |
| No | 16 (72.73) | 7 (63.64) | 9 (81.82) |
| Yes | 1 (4.55) | 1 (9.09) | 0 (0.0) |
| Missing | 5 (22.73) | 3 (27.27) | 2 (18.18) |
| **Coolness intensity (0-10)** | | | |
| Mean (SD) | 5.20 (2.80) | 4.64 (2.21) | 5.69 (3.31) |
| Median (IQR) | 5.00 (2.50-8.00) | 5.00 (2.50-6.00) | 5.50 (3.00-8.75) |
| Missing, n (%) | 7 (31.82) | 4 (36.36) | 3 (13.64) |
| **Coolness pain, n (%)** | | | |
| No | 11 (50.00) | 6 (54.55) | 5 (45.45) |
| Yes | 4 (18.18) | 1 (9.09) | 3 (27.27) |
| Missing | 7 (31.82) | 4 (36.36) | 3 (27.27) |
| **Temporal summation effect*** | | | |
| Mean (SD) | 13.31 (11.29) | 15.33 (10.31) | 11.57 (12.59) |
| Median (IQR) | 10.00 (6.00-16.00) | 12.50 (10.00-16.00) | 8.00 (2.00-20.00) |
| Missing, n (%) | 9 (40.91) | 5 (45.45) | 4 (36.36) |
| **Persistent pain after 10 stimuli, n (%)** | | | |
| No | 11 (50.00) | 8 (72.73) | 3 (27.27) |
| Yes | 4 (18.18) | 0 (0.0) | 4 (36.36) |
| Missing | 7 (31.82) | 3 (27.27) | 4 (36.36) |
| **Pressure pain threshold at neck (kg)** | | | |

31

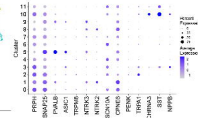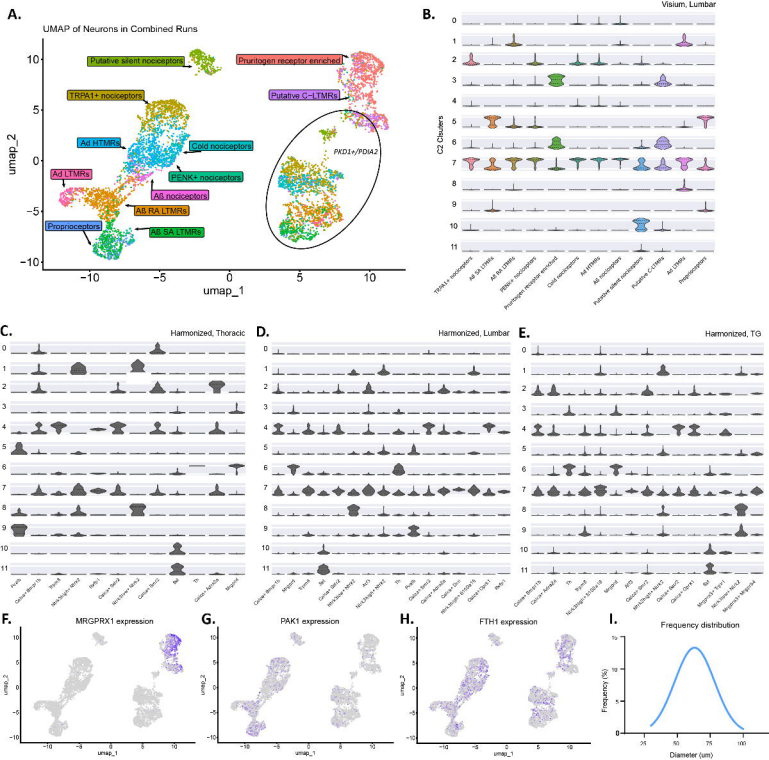| | | | |
|---|---|---|---|
| Mean (SD) | 9.27 (6.03) | 11.40 (4.10) | 7.50 (7.15) |
| Median (IQR) | 10.00 (5.00-15.00) | 10.00 (10.00-15.00) | 6.50 (2.00-10.00) |
| Missing, n (%) | 9 (40.91) | 5 (45.45) | 4 (36.36) |

1037

1038

1039 SD: standard deviation. IQR: Interquartile range. *Pain on both sides, with intensity on one side
1040 no more than 30% of the most painful side (otherwise categorized as bilateral). **Numerical
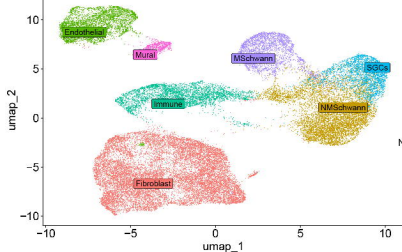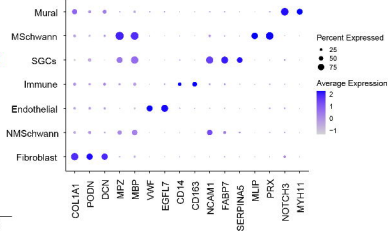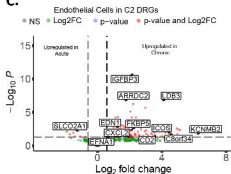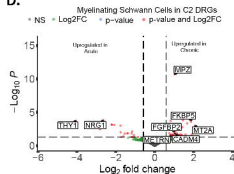1041 rating scale (0 = no pain, 10 = worst pain imaginable).

1042

1043

1044

**A.** UMAP Cells in the C2 DRG

**B.** SNAP25, PRPH, MPZ, MLIP, CD34, COL1A1, CD14, FABP7, CIDEA
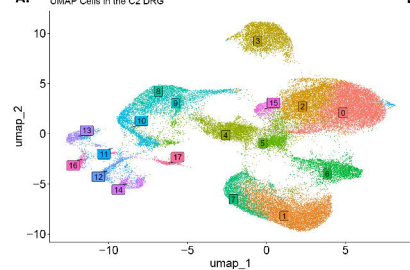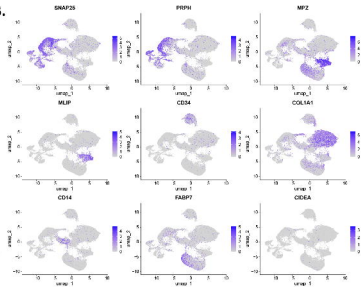
**C.** UMAP of Combined Runs
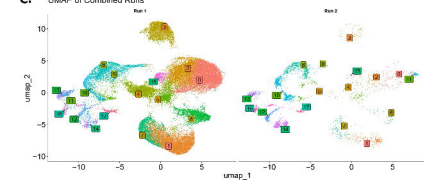
**D.** Expression of Marker Genes in Combined Runs
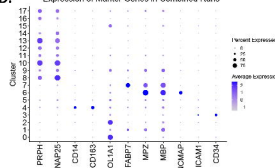
**E.** UMAP of Non-neuronal cells in Combined Runs
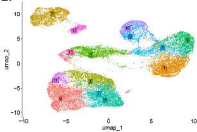
**F.** Expression of Marker Genes in Non-neuronal Cells in Combined Runs
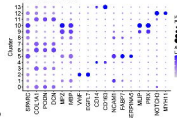
**G.** UMAP of Neurons in Combined Runs
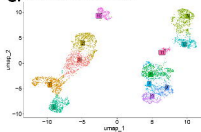
**H.** Expression of Marker Genes in Neurons in Combined Runs

A. UMAP of Neurons in Combined Runs

B. Visium, Lumbar

C. Harmonized, Thoracic

D. Harmonized, Lumbar

E. Harmonized, TG

F. MRGPRX1 expression

G. PAK1 expression

H. FTH1 expression

I. Frequency distribution

**A.** UMAP of Non-neuronal cells in Combined Runs

**B.** Expression of Marker Genes in Non-neuronal Cells in Combined Runs

**C.** Endothelial Cells in C2 DRGs

**D.** Myelinating Schwann Cells in C2 DRGs

**E.** Fibroblast Cells in C2 DRGs

# A.
## Differentially expressed genes identified with bulk RNAseq in C2 DRGs



# B.
## Differentially expressed genes in bulk and single-nucleus sequencing



| Gene | Bulk RNAseq | | Endothelial Cells single-nuc RNAseq | | Myelinating Schwann Cells single-nuc RNAseq | | Fibroblast Cells single-nuc RNAseq | |
|---|---|---|---|---|---|---|---|---|
| | Log2FC | adj p-value | Log2FC | adj p-value | Log2FC | adj p-value | Log2FC | adj p-value |
| C8orf34 | 0.019 | 0.504 | 4.533 | 0.017 | N/A | N/A | 1.836 | 0.011 |
| GADD45B | -0.014 | 0.518 | 1.753 | 0.000 | N/A | N/A | 1.901 | 0.008 |
| FGFBP2 | -0.020 | 0.442 | 0.056 | 0.685 | 1.020 | 0.008 | 1.886 | 0.001 |
| SLCO2A1 | -0.837 | 0.015 | -1.208 | 0.008 | N/A | N/A | 0.001 | 1.000 |
| KLF15 | 0.014 | 0.606 | 2.557 | 0.000 | 1.155 | 0.022 | 0.001 | 1.000 |
| FKBP5 | 0.003 | 0.807 | 2.058 | 0.005 | 1.887 | 0.000 | 0.000 | 1.000 |
| HSPA2 | -0.015 | 0.606 | 1.288 | 0.048 | 1.424 | 0.002 | 0.050 | 1.000 |
| SEC14L1 | 0.018 | 0.718 | 1.085 | 0.005 | 1.089 | 0.025 | -0.008 | 1.000 |

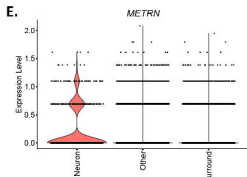## RNA expression in C2 DRGs measured with Visium spatial transcriptomics
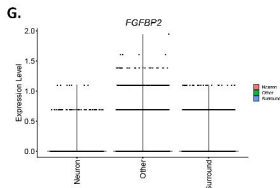
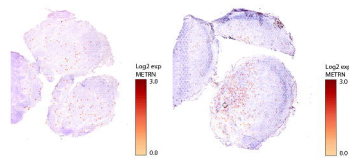## Normalized expression in sample 27 (acute)

## Normalized expression in sample 26 (chronic)



C. *SNAP25*

D. SNAP25 expression

E. *METRN*

F. METRN expression

G. *FGFBP2*

H. FGFBP2 expression

I. *SLCO2A1*

J. SLCO2A1 expression

**A.**

Upregulated ligand genes in non-neuronal cells → Upregulated receptor genes in neurons

Upregulated in endothelial cells
Upregulated in fibroblasts
Upregulated in myelinating Schwann cells
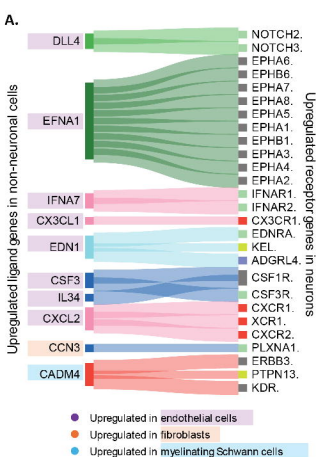
**Color Guide**
- cell adhesion
- cytokine
- cytoskeletal
- G-protein coupled receptor
- growth factor
- neuropeptide
- neurotrophic factor
- other intercellular signal
- other transmembrane signal receptor
- protein modifying enzyme
- tyrosine receptor kinase

**B.** Non-neuronal populations

**C.** Neuronal populations